



# Tumor cell-targeted delivery of CRISPR/Cas9 by aptamer-functionalized lipopolymer for therapeutic genome editing of VEGFA in osteosarcoma

Chao Liang <sup>a, b, c, d, \*\*, 1</sup>, Fangfei Li <sup>a, b, c, d, \*\*\*, 1</sup>, Luyao Wang <sup>a, b, c, d, 1</sup>, Zong-Kang Zhang <sup>e, 1</sup>, Chao Wang <sup>b, c, 1</sup>, Bing He <sup>b, c, d</sup>, Jie Li <sup>e</sup>, Zhihao Chen <sup>a</sup>, Atik Badshah Shaikh <sup>a, b, c, d</sup>, Jin Liu <sup>a, b, c, d</sup>, Xiaohao Wu <sup>a, b, c, d</sup>, Songlin Peng <sup>f</sup>, Lei Dang <sup>a, b, c, d</sup>, Baosheng Guo <sup>a, b, c, d</sup>, Xiaojuan He <sup>a, g</sup>, D.W.T. Au <sup>h</sup>, Cheng Lu <sup>g</sup>, Hailong Zhu <sup>a, b, c, \*\*\*\*</sup>, Bao-Ting Zhang <sup>e, \*\*\*\*\*</sup>, Aiping Lu <sup>a, b, c, d, g, i, \*\*\*\*\*</sup>, Ge Zhang <sup>a, b, c, d, \*</sup>

<sup>a</sup> Law Sau Fai Institute for Advancing Translational Medicine in Bone and Joint Diseases, School of Chinese Medicine, Hong Kong Baptist University, Hong Kong Special Administrative Region

<sup>b</sup> Institute of Integrated Bioinformedicine and Translational Science, School of Chinese Medicine, Hong Kong Baptist University, Hong Kong Special Administrative Region

<sup>c</sup> Institute of Precision Medicine and Innovative Drug Discovery, School of Chinese Medicine, Hong Kong Baptist University, Hong Kong Special Administrative Region

<sup>d</sup> Shenzhen Lab of Combinatorial Compounds and Targeted Drug Delivery, HKBU Institute of Research and Continuing Education, Shenzhen, China

<sup>e</sup> School of Chinese Medicine, Faculty of Medicine, Chinese University of Hong Kong, Hong Kong Special Administrative Region

<sup>f</sup> Department of Spine Surgery, Shenzhen People's Hospital, Ji Nan University Second College of Medicine, Shenzhen, China

<sup>g</sup> Institute of Basic Research in Clinical Medicine, China Academy of Chinese Medical Sciences, Beijing, China

<sup>h</sup> Department of Biology and Chemistry, City University of Hong Kong, Hong Kong Special Administrative Region

<sup>i</sup> Institute of Arthritis Research, Shanghai Academy of Chinese Medical Sciences, Shanghai, China

## ARTICLE INFO

### Article history:

Received 31 May 2017

Received in revised form

2 September 2017

Accepted 8 September 2017

Available online 13 September 2017

### Keywords:

Osteosarcoma

CRISPR/Cas9

VEGFA

Aptamer

In vivo delivery

## ABSTRACT

Osteosarcoma (OS) is a highly aggressive pediatric cancer, characterized by frequent lung metastasis and pathologic bone destruction. Vascular endothelial growth factor A (VEGFA), highly expressed in OS, not only contributes to angiogenesis within the tumor microenvironment via paracrine stimulation of vascular endothelial cells, but also acts as an autocrine survival factor for tumor cell themselves, thus making it a promising therapeutic target for OS. CRISPR/Cas9 is a versatile genome editing technology and holds tremendous promise for cancer treatment. However, a major bottleneck to achieve the therapeutic potential of the CRISPR/Cas9 is the lack of *in vivo* tumor-targeted delivery systems. Here, we screened an OS cell-specific aptamer (LC09) and developed a LC09-functionalized PEG-PEI-Cholesterol (PPC) lipopolymer encapsulating CRISPR/Cas9 plasmids encoding VEGFA gRNA and Cas9. Our results demonstrated that LC09 facilitated selective distribution of CRISPR/Cas9 in both orthotopic OS and lung metastasis, leading to effective VEGFA genome editing in tumor, decreased VEGFA expression and secretion, inhibited orthotopic OS malignancy and lung metastasis, as well as reduced angiogenesis and bone lesion with no detectable toxicity. The delivery system simultaneously restrained autocrine and

\* Corresponding author. Jockey Club School of Chinese Medicine Building, 7 Baptist University Road, Kowloon Tong, Hong Kong Special Administrative Region, China.

\*\* Corresponding author. Jockey Club School of Chinese Medicine Building, 7 Baptist University Road, Kowloon Tong, Hong Kong Special Administrative Region, China.

\*\*\* Corresponding author. Jockey Club School of Chinese Medicine Building, 7 Baptist University Road, Kowloon Tong, Hong Kong Special Administrative Region, China.

\*\*\*\* Corresponding author. Jockey Club School of Chinese Medicine Building, 7 Baptist University Road, Kowloon Tong, Hong Kong Special Administrative Region, China.

\*\*\*\*\* Corresponding author. Li Wai Chun Building, Chung Chi College, Chinese University of Hong Kong, Shatin, New Territories, Hong Kong Special Administrative Region, China.

\*\*\*\*\* Corresponding author. Jockey Club School of Chinese Medicine Building, 7 Baptist University Road, Kowloon Tong, Hong Kong Special Administrative Region, China.

E-mail addresses: liangchao@hkbu.edu.hk (C. Liang), fangfeili@hkbu.edu.hk (F. Li), hlzhu@hkbu.edu.hk (H. Zhu), zhangbaoting@cuhk.edu.hk (B.-T. Zhang), aipinglu@hkbu.edu.hk (A. Lu), zhangge@hkbu.edu.hk (G. Zhang).

<sup>1</sup> These authors contributed equally to this work.

paracrine VEGFA signaling in tumor cells and could facilitate translating CRISPR-Cas9 into clinical cancer treatment.

© 2017 Elsevier Ltd. All rights reserved.

## 1. Introduction

Osteosarcoma (OS) is a highly vascular and extremely destructive malignancy in children and adolescence [1,2]. The frequently occurred complications are distant metastasis (25–30%) [3] and pathologic fracture caused by bone destruction [4]. Lung is the most common metastatic site of OS [5]. Conventional treatment for OS is surgery in combination with chemotherapy [1,6]. However, the prognosis for OS patients who present with metastasis is significant worse [7,8]. Thus, it is urgent to develop novel treatment approaches for these patients.

Vascular endothelial growth factor A (VEGFA) is a classic angiogenic factor, which facilitates endothelial cell activation and new vessel formation [9]. Nevertheless, emerging evidence suggests that the function of VEGF is not limited to angiogenesis in tumor development [10]. In response to hypoxia, tumor cells produce and release VEGFA into tumor microenvironment [11]. On one hand, paracrine VEGFA from tumor cells stimulates endothelial cell-mediated angiogenesis to deliver oxygen and nutrients [12]. On the other hand, VEGFA also acts as an autocrine survival factor for tumor cell themselves [12]. Currently, it has been reported that VEGFA is highly expressed in OS cells and strongly associated with the poor prognosis of the patients [13]. Inhibition of VEGFA signaling suppressed OS growth, metastasis and angiogenesis [14–16], suggesting that VEGFA could be a novel therapeutic target for OS.

Clustered regularly interspaced short palindromic repeat (CRISPR)-associated Cas9 nuclease (CRISPR/Cas9) is a raising genome editing technology [17]. It is powered by the ease design of the guide RNAs (gRNAs) that direct Cas9 to the desired DNA locus for DNA cleavage [18]. Because of the high specificity and efficiency, CRISPR/Cas9 technology holds tremendous promise for cancer treatment [18–21]. However, a major bottleneck to achieve the therapeutic potential of the CRISPR/Cas9 is the lack of *in vivo* targeted delivery systems [22]. Aptamers, selected by cell-based systematic evolution of ligands by exponential enrichment (cell-SELEX), are single-stranded DNA (ssDNA) or RNA oligonucleotides [23]. They could specifically recognize target cells and have been widely used for *in vivo* targeted delivery of therapeutics, such as chemotherapy drugs and small interfering RNAs [24]. PEG-PEI-CHOL (PPC) lipopolymer, composed of polyethylenimine (PEI), methoxypolyethyleneglycol (PEG) and cholesterol (CHOL) which are covalent bound, has revealed its advantages in gene delivery such as large capacity and flexibility for sophisticated modifications [25–27]. In addition, PPC lipopolymer exhibits excellent safety on a phase II trial [28]. Thus, we hypothesized that an OS cell-specific aptamer could facilitate *in vivo* tumor-selective delivery of CRISPR/Cas9 encoding VEGFA gRNA and Cas9, leading to effective genome editing of VEGFA and inhibition of OS malignancy.

In this work, we screened an OS cell-specific aptamer (LC09) and constructed CRISPR/Cas9 plasmids encoding VEGFA gRNA and Cas9. Then, we encapsulated the CRISPR/Cas9 plasmids into PEG-PEI-Cholesterol (PPC) lipopolymer [29], which is a non-virus plasmid carrier under clinical trial [28], and conjugated the LC09 aptamer to PPC. We found that LC09 achieved tumor-specific delivery of CRISPR/Cas9 and facilitated VEGFA genome editing and inhibition of

orthotopic OS growth, lung metastasis, angiogenesis and bone lesion with no detectable toxicity in a syngeneic orthotopic OS mouse model. This demonstrates a novel CRISPR/Cas9-based genome editing approach for treatment of OS.

## 2. Materials and methods

### 2.1. Cell culture

Mouse OS cell line K7M2 (ATCC) was cultured in Dulbecco's modified Eagle's medium (DMEM, ATCC) supplemented with 10% fetal bovine serum (FBS) and 100 units ml<sup>-1</sup> penicillin-streptomycin. Mouse normal hepatocytes (AML12, ATCC) was cultured in a 1:1 mixture of DMEM and Ham's F12 medium supplemented with 0.005 mg ml<sup>-1</sup> insulin, 0.005 mg ml<sup>-1</sup> transferrin, 5 ng ml<sup>-1</sup> selenium, and 40 ng ml<sup>-1</sup> dexamethasone, as well as 10% FBS and 100 units ml<sup>-1</sup> penicillin-streptomycin. Human osteosarcoma cell line Saos2 (ATCC) was cultured in McCoy's 5A medium (ATCC) supplemented with 15% FBS and 100 units ml<sup>-1</sup> penicillin-streptomycin. Human liver cell line THLE-3 (ATCC) were cultured in BEGM (Lonza/Clonetics Corporation) supplemented with 5 ng ml<sup>-1</sup> EGF, 70 ng ml<sup>-1</sup> phosphoethanolamine and 10% FBS. Mouse and human PBMCs were obtained by density gradient separation with Ficoll-Paque PREMIUM (GE Healthcare Life Science) [30]. Mouse OS cell line K12 (CellBio, Shanghai) was cultured in DMEM supplemented with 10% FBS and 100 units ml<sup>-1</sup> penicillin-streptomycin. Mouse primary endothelial cells were purchased from Cell Biologics and cultured in Cell Biologics' growth medium and tested for expression of markers using antibodies for VECadherin (CD144, Santa Cruz) [31] or CD31/PECAM-1 (BD Biosciences) [32] by immunofluorescence staining or fluorescence-activated cell sorting (FACS). Human breast cancer cell line MBA-MD-231 (ATCC) was cultured in ATCC-formulated Leibovitz's L-15 medium supplemented with 10% FBS and 100 units ml<sup>-1</sup> penicillin-streptomycin. All the above cells were negative for bacteria, yeast, fungi and mycoplasma.

### 2.2. Synthesis of library, primers and aptamers

The ssDNA library contained 30 random nucleotides flanked by fixed regions 5'-GCAATGGTACGGTACTTCC-30nt-CAAAAGTG-CACGCTACTTGCTAA-3'. A forward primer (5'-GCAATGGTACGG-TACTTCC-3') and a reverse primer (5'-TTAGCAAAGTAGCGTGCACTTTG-3') were used in the PCR reaction for synthesis of double-stranded DNA (dsDNA) with equal length. The forward primer (5'-GCAATGGTACGGTACTTCC-3') and another reverse primer with a GC-rich reverse repeated sequence (underlined) at 5' terminus (5'-GCTAACGGGTGGACTTCCTAGTC-CACCCGTTAGCAAAGTAGCGTGCACTTTG-3') were used in the PCR reaction to generate ssDNA with unequal length strand [33]. The library, primers, aptamers and Rd sequence (TCCTAGTC-GAACGCTGGCTACTTAGCCATGGAACCTATTACCGTTGAA) with or without FAM were synthesized in Sangon Co Ltd, Shanghai, China.

### 2.3. Generation of ssDNA with unequal length strand

Using the above forward primer (5'-GCAATGGTACGGTACTTCC-

3') and reverse primer with a GC-rich reverse repeated sequence (underlined) at 5' terminus (5'-GCTAACGGGTGGGACTTCC-TAGTCCCACCCGTTAGCAAAGTAGCGTGCACTTTG-3') [34], PCR reaction was conducted in a 100  $\mu$ l mixture containing 10  $\mu$ l PCR buffer (10 $\times$ ), 0.2 mM dNTPs, 0.5  $\mu$ M each primer, 10 nM template and 2.5 U of Taq DNA polymerase (Takara). Thirty rounds of amplification were performed at 95 °C for 60 s, 37 °C for 30 s, and 58 °C for 40 s, followed by 5 min extension at 58 °C. ssDNA with unequal length was isolated from PCR products by electrophoresis in a 10% polyacrylamide-7M urea gel and the lower band of interest was purified from the gel for the next round of selection [34].

#### 2.4. Cell-SELEX

The synthetic ssDNA library (1500 pmol for initial round; 400 pmol for subsequent rounds) dissolved in 400  $\mu$ l binding buffer [PBS with 0.1 mg ml<sup>-1</sup> yeast tRNA (Sigma), 0.1 mg ml<sup>-1</sup> salmon sperm DNA (Invitrogen) and 1.0 mM MgCl<sub>2</sub> (Sigma)] was denatured by heating at 95 °C for 5 min and then cooled on ice for 10 min. The denatured library was incubated with 1–2  $\times$  10<sup>6</sup> target cells at 37 °C for 0.5–1 h (1 h for the first 6 cycles and 0.5 h for the left cycles). The cells were centrifuged and then washed with washing buffer [PBS with 1.0 mM MgCl<sub>2</sub> (Sigma)]. The cell-bound ssDNA was eluted by heating at 95 °C for 5 min and used as template for unequal length strand PCR reaction to generate the desired ssDNA. The negative selection was introduced from the second round of cell-SELEX. The enriched ssDNA pool was incubated with negative cells at 37 °C for 1 h. After centrifugation, the supernatant with cell-unbound ssDNA was desalting and amplified by unequal length strand PCR. After multiple rounds of selection, the final enriched ssDNA pool was PCR-amplified for the synthesis of dsDNA with equal length and cloned into pMD-18T vector (Takara) [35]. Cloned sequences were determined in Sangon Co Ltd, Shanghai, China. Secondary structures of aptamers were predicted by RNAstructure 5.6 software. Truncation was performed to remove the non-critical bases in fixed regions of each sequence based on the predicted secondary structures [33,34].

#### 2.5. Binding assay in cell-SELEX

FAM-labeled ssDNA library, enriched pools or aptamer candidates at the indicated concentrations were incubated with 2  $\times$  10<sup>5</sup> cells in 400  $\mu$ l binding buffer at 37 °C for 1 h. After washing, the cells were re-suspended in 400  $\mu$ l binding buffer. The mean fluorescence intensity was determined with a FACScan cytometer (BD Immunocytometry Systems) by counting 20,000 events. The equilibrium dissociation constants ( $K_d$ ) of the aptamer-cell interactions were calculated by the equation  $Y = B_{\max}X/(K_d + X)$  [36].

#### 2.6. Construction of CRISPR/Cas9 plasmids

Guide sequence oligos of 6 candidate gRNAs (Supplementary Table 2) targeting VEGFA were from GeCKOv2 libraries [37] and cloned into PX458 plasmids encoding Cas9 and gRNA scaffold. Non-sense gRNA (target sequence: GAACAGTCGGTTCGACT) was designed to have low homology to the human or murine genome and used as negative control [38]. Briefly, two complementary oligonucleotides with the guide oligos were annealed to generate dsDNA with overhangs on both ends and ligated to the *BbsI* pre-digested PX458 plasmids for generation of CRISPR/Cas9 plasmids. A G-C base pair was added at the 5' end of the guide sequence for U6 transcription, which did not adversely affect targeting efficiency. PX458 plasmids also contained markers including EGFP and an ampicillin resistance gene to aid the selection of the optimal gRNA

[39].

#### 2.7. Selection of the optimal VEGFA gRNA

K7M2 cells were seeded in 6-well plates, 25 cm<sup>2</sup> flasks or Nunc glass bottom dishes at appropriate densities and incubated overnight until 70%–80% confluence in DMEM supplemented with 10% FBS at 37 °C. The cells were transfected with different CRISPR/Cas9 plasmids in FBS-free DMEM using Lipofectamine 3000. After 8 h, the transfection medium was replaced with fresh DMEM supplemented with 10% FBS and the cells were cultured for an additional 48 h. To select the optimal VEGFA gRNA, Cas9 and EGFP expression was determined by western blotting and confocal imaging, respectively. Indels was examined by Surveyor assay [40] and confirmed by sequencing analysis [39]. Levels of VEGFA in both cell lysates and supernatants were tested by ELISA. Off-target sites were predicted by online CRISPR design tool (<http://crispr.mit.edu/>) and indels for the off-target sites were determined by Surveyor assay.

#### 2.8. Technological process of LC09-PPC-CRISPR/Cas9

(1) Synthesis of LC09-PEG2000-DSPE [36]: 3' thiol- and 2'-O-methyl-modified LC09 was activated in 100 mM Tris-(2-carboxyethyl) phosphine (TCEP) solution at 4 °C for 30 min, while lipids of DSPE-PEG2000-Mal were dissolved in chloroform, dried into a thin film and hydrated with 20 mM HEPES buffer (pH 6.5). Then, the freshly prepared LC09 was added to DSPE-PEG2000-Mal solution at an aptamer/lipid molar ratio of 1: 5. The coupling reaction was performed overnight at 4 °C with gentle stirring. Purification was performed by ultracentrifugation (10,000 g, 15 °C, 15 min) in centrifugal filter tubes (MWCO 10,000). (2) Synthesis of PEG-PEI-Cholesterol (PPC)-CRISPR/Cas9 [41]: The PPC was prepared by combining branched polyethylenimine (BPEI, MW 1800) with cholestryl chloroformate and activated methoxypolyethyleneglycol (MPEG-SPA, methoxypolyethyleneglycol-propionic acid N-hydroxysuccinimidyl ester, MPEG MW 550, ester MW 719). The BPEI was dissolved into dry chloroform. The solution containing cholestryl chloroformate and mPEG550-SPA in dry chloroform was added dropwise to the freshly dissolved BPEI solution with stirring over 20–30 min, followed by a 3–4 h incubation period. The molar ratio of PEI/PEG/Cholesterol is 1: 2: 1. The mixture was then placed under vacuum to concentrate the solution and remove the residual chloroform. The resulting PPC complex was dissolved in 1 M aqueous HCl. Then the PPC hydrochloride solution was again concentrated under vacuum, yielding a highly viscous material. To isolate the PPC hydrochloride and remove unreacted starting materials from products, the concentrated mixture was mixed with acetone (<0.4% water) and stirred leading to PPC hydrochloride precipitation as a free-flowing material. Following precipitation, the supernatant liquid was discarded. The washing step was repeated to ensure complete removal of residual reaction. PPC-CRISPR/Cas9 complexes were generated by firstly preparing PPC and CRISPR-Cas9 plasmids at appropriate concentrations in 10% lactose respectively. The plasmids solution was then added dropwise with stirring to the PPC solution at the nitrogen of PPC/phosphate of plasmids (N/P) molar ratio of 11: 1 and incubated for 15 min at room temperature to form the complexes. The PPC-CRISPR/Cas9 complexes were purified by size exclusion chromatography on a Sepharose CL-4B column using HBS (pH 7.4) as the running buffer to remove free plasmids, and chemical reagents [22]. (3) Insertion of aptamer into the surface of PPC-CRISPR/Cas9 and purification: LC09-PEG2000-DSPE was added to the PPC-CRISPR/Cas9 suspension and incubated in a water bath at 37 °C overnight. Then, LC09-PPC-CRISPR/Cas9 was purified by size

exclusion chromatography on a Sepharose CL-4B column, using HBS (pH 7.4) as a running buffer to remove unconjugated micelles and chemical reagents [36].

### 2.9. In vitro characterization of LC09-PPC-CRISPR/Cas9

(1) Encapsulation efficiency: The encapsulation efficiency of CRISPR/Cas9 plasmids was calculated according to the formula:  $(A_{\text{total}} - A_{\text{free}})/A_{\text{total}} \times 100\%$ .  $A_{\text{total}}$  means the amount of the CRISPR/Cas9 plasmids added into PPC solution.  $A_{\text{free}}$  means the amount of free CRISPR/Cas9 plasmids in running buffer after purification of PPC-CRISPR/Cas9 by Sepharose CL-4B column. The amount of plasmids was determined by UV–Vis spectrophotometer (Nano-Drop 2000; Thermo Scientific) [42]. (2) Loading efficiency of aptamers: To determine the loading efficiency of LC09, LC09 was labeled with Cy5 at 5' terminus and used for synthesis of LC09-PEG2000-DSPE. After addition of LC09-PEG2000-DSPE to the PPC-CRISPR/Cas9 suspension, fluorescence intensity in the mixture was determined by a microplate reader (Bioscan, Washington, DC) and expressed as  $F_{\text{total}}$ . LC09-PPC-CRISPR/Cas9 was purified by size exclusion chromatography and running buffer was collected for concentration. Fluorescence intensity in running buffer with unconjugated LC09-PEG2000-DSPE was determined and expressed as  $F_{\text{free}}$ . The loading efficiency of LC09 was calculated by the formula:  $(F_{\text{total}} - F_{\text{free}})/F_{\text{total}} \times 100\%$  [36]. (3) Particle size and zeta potential: The hydrodynamic diameters and zeta potentials of LC09-PPC-CRISPR/Cas9 were measured by laser light scattering using a Delsa™ Nano HC Particle Analyzer (Beckman Coulter Corporation, USA) at 25 °C following dilution with distilled water [36]. (4) The morphology of LC09-PPC-CRISPR/Cas9: The morphology was observed by Cryo-transmission electron microscopy (cryo-TEM). 10 µl LC09-PPC-CRISPR/Cas9 suspension was placed on a copper grid covered by a holey carbon film. Excess sample was blotted with filter paper, and the grid was rapidly plunged into liquid ethane (cooled to approximately –180 °C with liquid nitrogen) in a cryo-box (Carl Zeiss NTS GmbH, D-Oberkochen). The frozen specimen was then transferred via a cryo-transfer unit (Gatan 626-DH) to a transmission electron microscope (FEI/Philips Tecnai 12 Bio TWIN) with a pre-cooled cryo-specimen holder [36]. (5) Serum stability: Serum stability of 3' thiol- and 2'-O-methyl-modified LC09 and CRISPR/Cas9 plasmids encapsulated in PPC were assessed by electrophoresis at 0, 2, 4, 6, 12, and 24 h. Briefly, 3' thiol- and 2'-O-methyl-modified LC09 and PPC-CRISPR/Cas9 were incubated with 50% FBS at 37 °C. After 0, 2, 4, 6, 12 and 24 h, PPC-CRISPR/Cas9 sample was treated with dextran sulfate for decomplexation. 3' thiol- and 2'-O-methyl-modified LC09 sample and PPC-CRISPR/Cas9 sample with decomplexation were loaded onto 2% agarose gels for electrophoresis. The free LC09 aptamer and CRISPR/Cas9 plasmids served as negative controls [36].

### 2.10. Cellular uptake of different CRISPR/Cas9 formulations

OS cells were seeded in 6-well plates at appropriate densities and cultured overnight until 70%–80% confluence in DMEM supplemented with 10% FBS at 37 °C. The cells were incubated with different Cy5-labeled CRISPR/Cas9 formulations in FBS-free DMEM including PPC-CRISPR/Cas9, Rd-PPC-CRISPR/Cas9, LC09-PPC-CRISPR/Cas9 and Lipo 3000-CRISPR/Cas9, respectively. After 8 h, the cells were washed and re-suspended in 400 µl PBS. Fluorescence was determined with a FACScan cytometer (BD Immunocytometry Systems) by counting 20,000 events. OS cells without any incubation were performed as a blank control to measure background signals, which were subtracted from the final calculations [36].

### 2.11. In vitro treatment of OS cells with different CRISPR/Cas9 formulations

OS cells were seeded in 6-well plates, 96-well plates, 25 cm<sup>2</sup> flasks or Nunc glass bottom dishes (Thermo Fisher Scientific) at appropriate densities and cultured overnight until 70%–80% confluence in DMEM supplemented with 10% FBS at 37 °C. The cells were incubated with vehicle (PBS) or different CRISPR/Cas9 formulations in FBS-free medium. After 8 h, the medium was replaced with fresh medium supplemented with 10% FBS and the cells were continuously cultured to determine CRISPR/Cas9 expression, genome editing, cell viability, migration and invasion.

### 2.12. Preparation of conditioned medium from OS cells

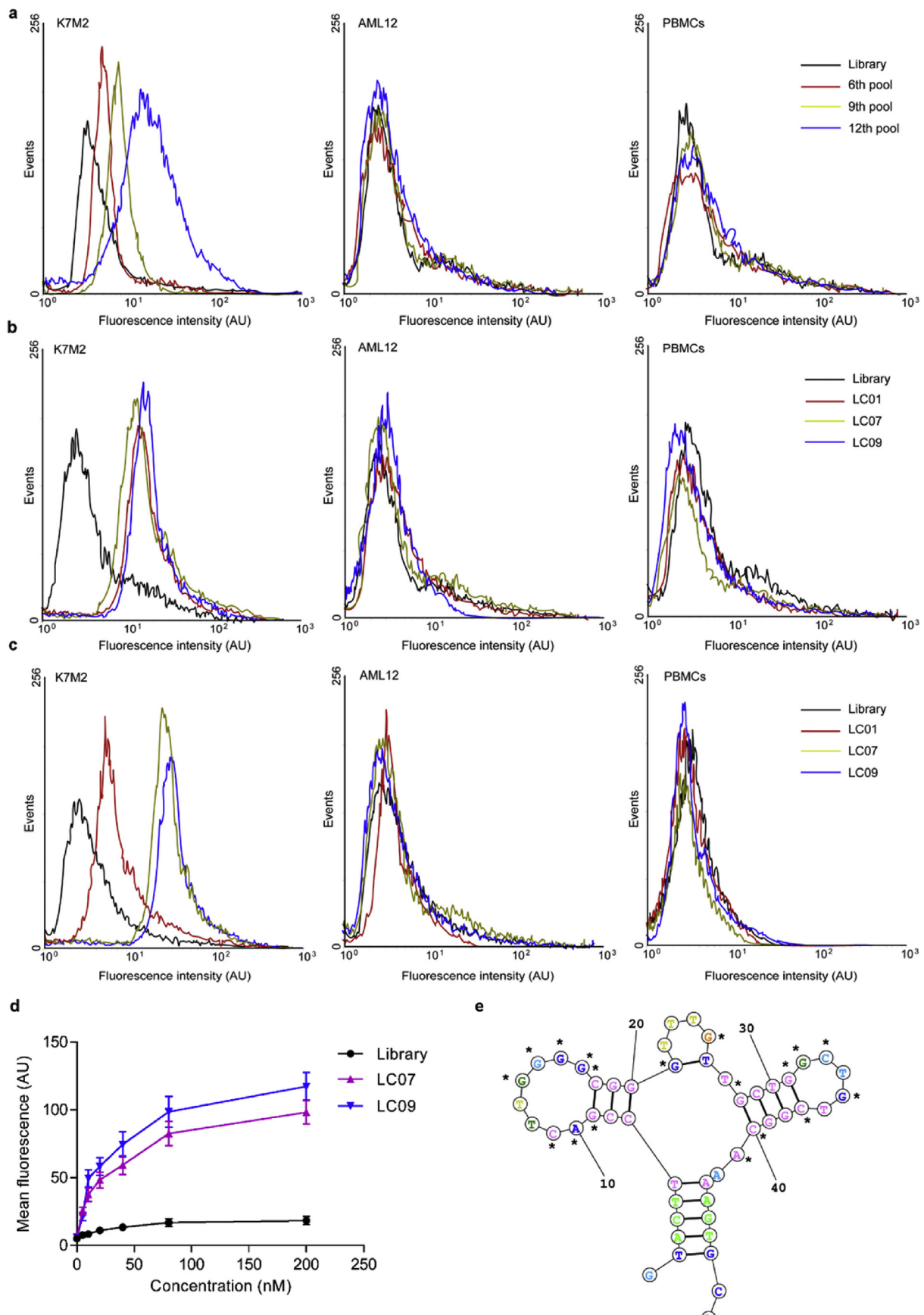
OS cells were seeded in 75 cm<sup>2</sup> flasks at appropriate densities and incubated overnight until 70%–80% confluence in medium supplemented with 10% FBS at 37 °C. The cells were incubated with vehicle (PBS) or different CRISPR/Cas9 formulations in FBS-free medium including PPC-CRISPR/Cas9, Rd-PPC-CRISPR/Cas9, LC09-PPC-CRISPR/Cas9 and LC09-PPC-CRISPR/Cas9 Ctrl, respectively. After 8 h, the medium was replaced with fresh medium supplemented with 10% FBS and the cells were cultured for an additional 48 h. Then, the conditioned medium was collected for culturing mouse primary endothelial cells or aortic ring assay.

### 2.13. Transwell invasion assay in vitro

Invasion assays were performed using 24-Multiwell Insert System (Corning BioCoat™ Matrigel Invasion Chamber with 8.0 µm PET membrane) as described in the manufacturer's protocol. For invasion of OS cells treated with vehicle (PBS) or different CRISPR/Cas9 formulations, the cells were transferred on the top of Matrigel-coated invasion chambers and cultured with DMEM supplemented with 1% FBS for 48 h. DMEM supplemented with 10% FBS was added to the lower chambers. For invasion of primary endothelial cells, the cells were incubated with conditioned medium from OS cells on the top of Matrigel-coated invasion chambers for 48 h. Endothelial cell growth medium was added to the lower chambers. Invaded cells on the lower surface of Matrigel-coated invasion chambers were stained with crystal violet stain and observed under a light microscope [43].

### 2.14. Western blotting

Whole proteins were extracted from OS cell lysates, OS cell supernatants, OS tissues, livers and lung metastatic sites and the protein concentrations were determined by protein assay reagent (Bio-Rad). Subsequently, the total proteins (40 µg per well) were separated with 10% SDS-PAGE and transferred to polyvinylidene difluoride membranes (Millipore). After blocked 1 h with 5% milk in Tris-buffered saline and Tween 20 (TBST; 20 mM Tris-HCl, pH 7.5, 150 mM NaCl, and 0.5% Tween 20), the membranes were incubated with anti-Cas9 polyclonal antibody (Abcam) or anti-β-actin monoclonal antibody (Santa Cruz Biotechnology) at 4 °C overnight. After washed three times with TBST, the membranes were incubated with horseradish peroxidase (HRP)-labeled secondary antibody (Invitrogen) for 1 h at room temperature. Finally, the membranes were washed three times with TBST and then detected with enhanced chemiluminescence reagents (Pierce) and visualized with ChemiDoc™ Touch Imaging System (Bio-Rad Laboratories).



### 2.15. Wound healing assay

For migration of OS cells treated with vehicle (PBS) or different CRISPR/Cas9 formulations, a wound area was carefully created by scraping the cell monolayer with a sterile 10  $\mu$ l pipette tip. After being washed three times with PBS, scratches were photographed as the baseline. Subsequently, the cells were cultured in DMEM supplemented with 10% FBS for another 48 h. For migration of endothelial cells, the cells were seeded in 6-well plates at appropriate densities and cultured overnight until 70%–80% confluence in endothelial cell growth medium at 37 °C. A wound area was carefully created by scraping the cell monolayer with a sterile 10  $\mu$ l pipette tip. After being washed three times with PBS, scratches were photographed as the baseline. Then, the endothelial cell growth medium was changed to conditioned medium from OS cells and cultured for another 18 h. The width of the wound area was monitored with an inverted microscope [43].

### 2.16. CCK-8 assay

Cell viability of OS cells and proliferation of endothelial cells were examined by the CCK-8 (Beyotime Inst Biotech) according to manufacturer's instructions. For OS cells, 5  $\times$  10<sup>3</sup> cells per well were seeded in 96-well plates and cultured for 24 h. Then, the cells were treated with vehicle (PBS) or different CRISPR/Cas9 formulations. For endothelial cells, 5  $\times$  10<sup>3</sup> cells per well were seeded in 96-well plates and cultured for 24 h. Then, the cells were treated with different conditioned medium from OS cells. After 48 h, 10  $\mu$ l WST-8 dye was added to each well and the cells were incubated at 37 °C for 3 h and the absorbance was determined at 450 nm using a microplate reader [44].

### 2.17. Surveyor assay

OS cells were treated with different CRISPR/Cas9 as described above. Cells were incubated at 37 °C for 48 h post treatment before genomic DNA extraction. Genomic DNA was extracted using the QuickExtract DNA extraction kit (Epicentre) following the manufacturer's protocol. Briefly, cells were resuspended in QuickExtract solution and incubated at 65 °C for 15 min and 98 °C for 10 min. Genomic region surrounding the CRISPR target site for each gene was PCR amplified using the primers in Supplementary Table 6 and products were purified using QiaQuick Spin Column (Qiagen) following manufacturer's protocol. A total of 400 ng purified PCR products were mixed with 2  $\mu$ l 10  $\times$  Taq polymerase PCR buffer (Enzymatics) and ultrapure water to a final volume of 20  $\mu$ l and subjected to a re-annealing process to enable heteroduplex formation: 95 °C for 10 min, 95 °C to 85 °C ramping at –2 °C/s, 85 °C to 25 °C (at –0.25 °C/s) and 25 °C hold for 1 min. After reannealing, products were treated with Surveyor nuclease and Surveyor Enhancer S (Transgenomics) following the manufacturer's recommended protocol, and analyzed on 4–20% Novex TBE polyacrylamide gels (Life Technologies). Gels were stained with SYBR Gold DNA stain (Life Technologies) for 30 min and imaged with a Gel Doc gel imaging system (Biorad). Quantification was based on relative band intensities. Indel percentage was determined by the

formula,  $100 \times (1 - (b + c)/(a+b + c))1/2$ , where a is the integrated intensity of the undigested PCR product, and b and c are the integrated intensities of each cleavage product [45].

### 2.18. Labeling of CRISPR/Cas9 plasmids with Cy5

CRISPR/Cas9 plasmids were labeled with Cy5 using the Label IT® Tracker™ intracellular nucleic acid localization kit (Mirus Bio LLC) according to manufacturer's instructions. Briefly, the Label IT® Tracker™ Reagent and Tracker Reconstitution Solution were warmed to room temperature. The Label IT® Reagent were centrifuged to collect the dried pellet and added into 50  $\mu$ l pre-warmed Tracker Reconstitution Solution. Plasmid labeling reaction components including 37.5  $\mu$ l DNase-, RNase-free (molecular biology-grade) water, 5  $\mu$ l 10  $\times$  Labeling Buffer A, 5  $\mu$ l 1 mg/ml nucleic acid sample and 2.5  $\mu$ l Label IT® Reagent were incubated at 37 °C for 1 h. Labeled plasmids were purified using ethanol precipitation and stored at –20 °C, protected from light [46].

### 2.19. Confocal imaging for endocytosis pathways

K7M2 cells were seeded in Nunc glass bottom dishes (Thermo Fisher Scientific) at appropriate densities and cultured overnight until 50% confluence in DMEM supplemented with 10% FBS at 37 °C. The cells were incubated with different CRISPR/Cas9 formulations in FBS-free DMEM for 4 h. Alexa Fluor 448-labeled endocytic markers (250  $\mu$ g ml<sup>–1</sup> dextran, 10  $\mu$ g ml<sup>–1</sup> cholera toxin-B or 50  $\mu$ g ml<sup>–1</sup> transferrin) were added during the final 30 min of the incubation. The cells were washed and counterstained with 1  $\mu$ g ml<sup>–1</sup> Hoechst 33342 (Thermo Fisher Scientific) and analyzed by confocal microscopy [36].

### 2.20. Chemical inhibition of endocytosis pathways

K7M2 cells were seeded in 25 cm<sup>2</sup> at appropriate densities and cultured overnight until 70–80% confluence in DMEM supplemented with 10% FBS at 37 °C. Then chemical inhibitors of macropinocytosis (EIPA or cytochalasin D) or inhibitors of caveolae-mediated endocytosis (dynasore or chlorpromazine) were pre-incubated with K7M2 cells at 37 °C for 0.5 h before the addition of LC09-PPC-CRISPR/Cas9 plasmids. After 4 h, the cells were washed twice and re-suspended in 400  $\mu$ l of PBS. Fluorescence of Cy5-labeled CRISPR/Cas9 was determined with a FACScan cytometer (BD Immunocytometry Systems) by counting 20,000 events [36].

### 2.21. In vitro tube formation assay

Mouse primary endothelial cells were seeded in 12-well plates coated with Geltrex (Thermo Fisher Scientific) at appropriate densities and cultured in conditioned medium from OS cells treated with vehicle (PBS) or different CRISPR/Cas9 formulations. After 12 h, the cells were stained with calcein AM (Life Technologies) and analyzed by fluorescent microscopy (Eclipse TE300; Nikon) [42].

**Fig. 1. Screening of osteosarcoma (OS) cell-specific aptamers by Cell-SELEX.** (a) Binding ability of the enriched FAM-labeled ssDNA pools to target cells (mouse OS cells K7M2) and negative cells (mouse normal hepatocytes AML12 and PBMCs) as determined by flow cytometry. The concentration of the enriched pools in the binding buffer was 200 nM. Nonspecific binding was measured using an FAM-labeled unselected ssDNA library. AU, arbitrary units; events, number of cells with the given fluorescence intensity. (b) Flow cytometric analysis of binding ability of the FAM-labeled aptamer candidates (LC01, LC07 and LC09) to K7M2 cells, AML12 cells and PBMCs. (c) Binding ability of the FAM-labeled, 2'-O-methyl-nucleotide substitutions-modified aptamer candidates (LC01, LC07 and LC09) to K7M2 cells, AML12 cells and PBMCs as determined by flow cytometry. (d) Flow cytometric analysis to determine the binding affinity of LC07 and LC09 aptamers for K7M2 cells.  $K_d$  (LC07) = 24.05 nM;  $K_d$  (LC09) = 22.92 nM. The concentrations of LC07 and LC09 ranged from 5 nM to 200 nM. The data are presented as the mean  $\pm$  sd;  $n$  = 3 per group. (e) Proposed secondary structure of LC09. 2'-O-methoxy nucleotides were marked with the asterisk symbol (\*). Thick lines, hydrogen bonds between base pairs; thin lines, main phosphodiester bond. PBMCs, peripheral blood mononuclear cells.

## 2.22. Animal handing

All the animals were housed in Laboratory Animal House of the Law Sau Fai Institute for Advancing Translational Medicine in Bone & Joint Diseases with a temperature-controlled, 12 h light/dark cycle facility, and food and water were available ad libitum. The animals were acclimatized to the laboratory conditions for at least 7 d before being used in experiments. The animals were anesthetized by Ketamine (100 mg kg<sup>-1</sup>) and Xylazine (10 mg kg<sup>-1</sup>) during cell inoculation, X-ray analysis and Matrigel injection. For each *in vivo* study, the animals were euthanized by lethal dose of pentobarbital after treatment. The animal study procedures were approved by the Animal Experimentation Ethics Committee of the Hong Kong Baptist University (Ref. No.: HASC/12–13/0032).

## 2.23. Ex vivo aortic ring assay

Thoracic aortas were harvested from 2-month-old healthy male BALB/c mice and the surrounding tissues were dissected out. Aortic ring assay was performed as previously described. Briefly, 0.5 mm long rings were excised from the aortas and submerged in 350 ml Matrigel (phenol red-free; BD Biosciences) in 24-well plates. The rings were incubated with conditioned medium from K7M2 cells treated with vehicle (PBS) or different CRISPR/Cas9 formulations at 37 °C. The medium was changed every 2 d. After 10 d of incubation, vascular sprouting from the aortas were photographed under a light microscope (Olympus Inc., Center Valley, PA) [47].

## 2.24. Syngeneic orthotopic OS mouse model

To establish a syngeneic orthotopic OS mouse model, 2-month-old healthy male BALB/c mice received intratibial inoculation of OS cells (K7M2). Briefly, K7M2 cells were harvested and suspended in PBS at 4 °C. The mice were anesthetized with Ketamine (100 mg/kg) and Xylazine (10 mg/kg). Left hindlimbs were shaved and cleaned with 75% ethanol. The knees of the mice were flexed beyond 90° and the cortex of proximal tibial crest were penetrated using 25 gauge needles by a rotating action. Once the tibial bone cortex was penetrated, the needles were further inserted 2 mm down the diaphysis, followed by injection of 10 µl K7M2 cells ( $5 \times 10^5$ ) into the tibia. The mice were weekly monitored by the Faxitron MX-20 X-ray machine (Faxitron X-ray Corporation) [48].

## 2.25. Biophotonic imaging analysis

Fluorescence imaging of the Cy5-labeled CRISPR/Cas9 distribution and EGFP expression of CRISPR/Cas9 in tissues was performed using an IVIS® Lumina XR imaging system (Xenogen Imaging Technologies). Constant illumination settings, including exposure time (5 s), binning factor (4), f-stop (2) and field of view (15 cm for both width and length), were used during all image acquisition. Fluorescent and photographic images were acquired and overlaid. The pseudo-color image represented the spatial distribution of photon counts within the tissues. Background fluorescence recorded under a background filter (410–440 nm) was subtracted prior to the analysis [36].

## 2.26. Immunofluorescence staining

OS tissues and tumor lung metastatic sites were dissected from mice and embedded in optimal cutting temperature medium (O.C.T.). The cryosection (thickness: 5 µm) were cut in a freezing cryostat at –20 °C. The sections were air dried at room temperature, fixed in ice-cold acetone for 10 min, permeabilized with 0.3% Triton X-100 at room temperature for 20 min and blocked in 1%

BSA. The sections were then incubated overnight at 4 °C with a rabbit polyclonal antibody to Ezrin (Abcam). Following three washes in PBS, the sections were incubated with Alexa Fluor® 488-conjugated donkey anti-rabbit IgG (Abcam) for 1 h. The sections were mounted with medium containing DAPI (Abcam) and examined under a fluorescence microscope (Q500MC Leica image analysis system). H&E staining was performed on the adjacent sections for orientation [36].

## 2.27. Immunohistochemistry

OS tissues and metastatic lungs dissected from mice were fixed with formalin and paraffin-embedded. Immunohistochemical analyses were performed on 4 µm paraffin sections were deparaffinized using xylene and rehydrated in a series of decreasing concentrations of ethanol solutions. Heat-induced epitope retrieval was carried out in citrate buffer (10 mM sodium citrate, pH 6.0) in a pressure cooker for 4 min. Endogenous peroxidase was blocked using a 3% hydrogen peroxide solution for 20 min. The slides were washed with PBS and incubated with primary antibodies overnight at 4 °C. Primary antibodies including a rabbit polyclonal antibody to VEGFA, a rabbit monoclonal antibody to Ki67, a rabbit polyclonal antibody to Ezrin, a rabbit polyclonal antibody to MMP9 and a rabbit polyclonal antibody to Survivin were from Abcam. After washing for three time, the sections were then incubated with HRP-labeled second antibody for 1 h at room temperature. Colored reactions were developed using diaminobenzidine (DAB) as chromogenic substrate, while nuclear contrast was achieved using Harris hematoxylin counterstaining. Sections were visualized in a Leica DM6000 Digital microscope. For Immunohistochemical analyses of vWF and CD34, in OS tissues, a rabbit polyclonal antibody to vWF and a rabbit monoclonal antibody CD34 from Abcam were used according to the above protocol [49].

## 2.28. X-ray analysis

During the treatment period, mice were anesthetized and placed in a prone position. Digital radiography of the OS-bearing hindlimbs were carried out using the Faxitron MX-20 X-ray machine (Faxitron X-ray Corporation). Digital X-ray images of the mice were collected for 8 s at 35 kV once a week. Volume of OS tissues were calculated by the formula: volume = (width)<sup>2</sup> x length/2, with subtraction of normal tissue volume of the contralateral non-tumor hindlimb [50].

## 2.29. Matrigel plug assay

Matrigel plug assay was conducted 10 d before the mice were euthanized. Briefly, the mice were anesthetized and 200 µl liquid Matrigel matrix (phenol red-free; BD Biosciences) containing heparin (50 units/ml) was subcutaneously injected in OS region. After the treatment, the Matrigel plugs were removed and photographed [51].

## 2.30. MicroCT analysis

The OS-bearing hindlimbs of mice from each group were scanned *ex vivo* with a microCT system (vivaCT 40, SCANCO MEDICAL, Switzerland). The calibration was performed routinely in our lab using phantom according to the manufacturer's recommendations. The OS-bearing hindlimbs were placed into a plastic cylindrical holder, positioned along the scanning axis, and the ankle was fixed to avoid movements during scanning. In total, 844 slices with a voxel size of 10 mm were scanned for the whole OS-bearing hindlimbs. Bone destruction of the trabecular bone was analyzed after

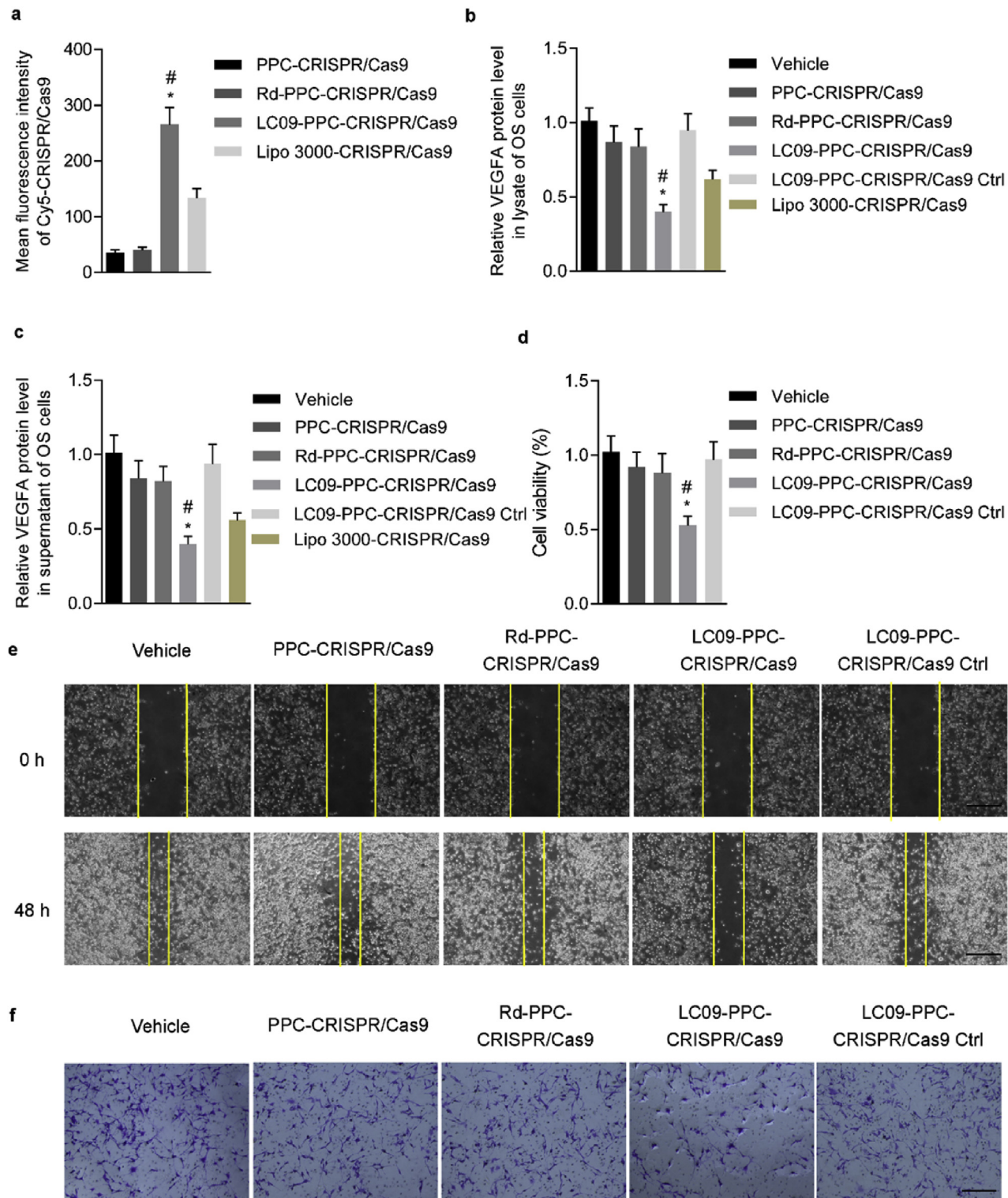
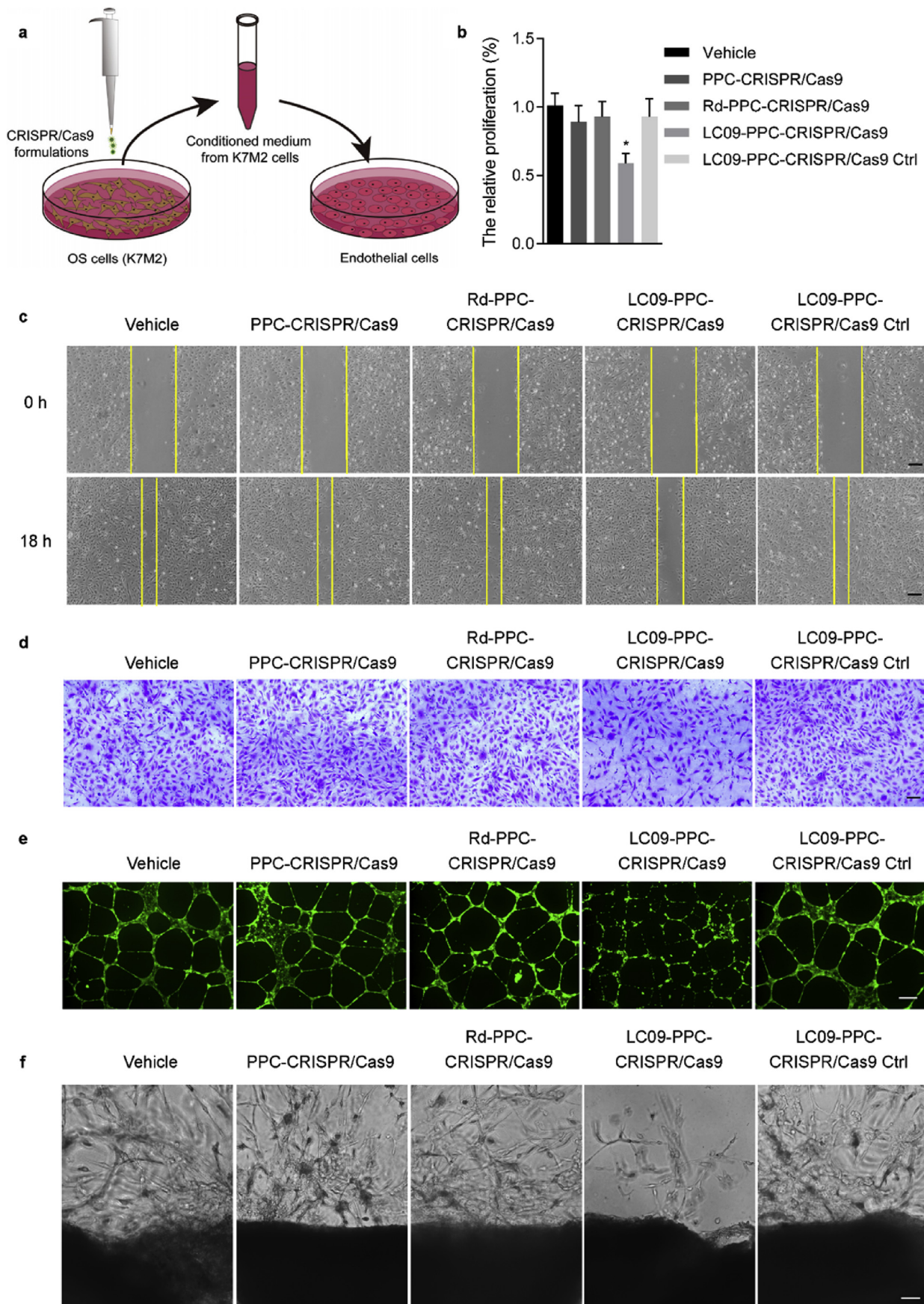


**Fig. 2. In vitro cellular uptake, genome editing and anti-tumor activity of different CRISPR/Cas9 formulations.** (a) Flow cytometric analysis to determine the mean fluorescence intensity of Cy5-labeled CRISPR/Cas9 plasmids in OS cells (K7M2) treated with PPC-CRISPR/Cas9, Rd-PPC-CRISPR/Cas9, LC09-PPC-CRISPR/Cas9 and Lipo 3000-CRISPR/Cas9, respectively. (b) Levels of VEGFA protein in lysates of K7M2 cells treated with vehicle (PBS) or different CRISPR/Cas9 formulations. (c) Levels of VEGFA protein in supernatants of K7M2 cells treated with vehicle (PBS) or different CRISPR/Cas9 formulations. VEGFA protein levels were determined by enzyme-linked immunosorbent assay (ELISA) and normalized to those in vehicle group. (d) Viability of K7M2 cells treated with vehicle (PBS) or different CRISPR/Cas9 formulations, as determined by Cell Counting Kit-8 (CCK-8) assay. The data are presented as the mean  $\pm$  sd; \* $P < 0.05$ ; # $P < 0.05$ . One-way ANOVA with a post-hoc test was performed and the statistical differences between the two groups were determined by the Student's *t*-test. (e) Wound healing assay to determine the migration of K7M2 cells treated with vehicle (PBS) or different CRISPR/Cas9 formulations. Wound width was indicated by two yellow dotted lines. Scale bars, 200  $\mu$ m. (f) Invasion of K7M2 cells treated with vehicle (PBS) or different CRISPR/Cas9 formulations, as examined by transwell invasion assay and crystal violet staining. Scale bars, 1000  $\mu$ m.  $n = 3$  per group. The CRISPR/Cas9 plasmids encoded gRNA 2, while the CRISPR/Cas9 Ctrl plasmids encoded a non-sense gRNA. Rd, a random sequence served as a negative control of LC09 aptamer; Lipo 3000, Lipofectamine 3000.



three-dimensional reconstruction (sigma = 1.2, supports = 2 and threshold = 180) [36].

### 2.31. Enzyme-linked immunosorbent assay (ELISA)

VEGFA in OS cell lysates, supernatants, OS tissues and lung metastatic sites were determined by VEGFA ELISA kits from Abcam, according to the manufacturer's instructions.

### 2.32. Biochemical and hematological assays

Blood samples were collected from mice after treatment with LC09-PPC-CRISPR/Cas9 or vehicle (PBS). Serum biochemical parameters including alanine transaminase (ALT), aspartate transaminase (AST) and blood urea nitrogen (BUN) were analyzed by a Vitros 250 Analyzer (Ortho Clinical Diagnostics). Hematological parameters including red blood cell (RBC), haemoglobin (HGB), hematocrit (HCT), white blood cell (WBC) and platelets (PLT) were determined by the fully automated ABX Pentra 60C + Analyzer (Horiba ABX) [36].

### 2.33. Statistical analyses

All numerical data are expressed as the mean  $\pm$  standard deviation. Statistical differences among groups were analyzed by one-way analysis of variance with a *post-hoc* test to determine group differences in the study parameters. All statistical analyses were performed with SPSS software, version 22.0. Statistical differences between two groups were determined by the Student's *t*-test.  $P < 0.05$  was considered statistically significant. All the statistical data in this project were analyzed by a contract service from Bio-informedicine (San Diego, CA, USA). We chose the representative images based on the average/median level of the data for each group. For the *in vivo* experiments, sample size was pre-determined by a power calculation. The mice were grouped randomly and blindly to researchers. The mice in poor body condition before the experiments were excluded.

## 3. Results

### 3.1. Screening of OS cell-specific aptamers by cell-SELEX

We used highly metastatic mouse OS cells (K7M2) [52] as target cells to screen aptamers by cell-SELEX from a library composed of  $10^{15}$  different ssDNA. Mouse normal hepatocytes (AML12) and peripheral blood mononuclear cells (PBMCs) were chosen as negative cells with the purpose of reducing non-specific liver and PBMCs uptake after *in vivo* administration [36]. With increasing rounds of selection, we observed progressively enhanced fluorescence intensity of fluorescein amidite (FAM)-labeled ssDNA pools in K7M2 cells by flow cytometric analysis, whereas no obvious change of fluorescence intensity was found in AML12 cells and PBMCs (Fig. 1a). After 12 rounds of selection, we sequenced the highly

enriched ssDNA pool and chose twenty representative sequences (from 200 clones), on the basis of their predicted secondary structures, for truncation to remove the non-critical bases [53] (Supplementary Table 1). Flow cytometric analysis showed that three aptamer candidates (LC01, LC07 and LC09) had good binding ability to K7M2 cells rather than AML12 cells, PBMCs (Fig. 1b). To minimize nuclease degradation, the aptamer candidates were modified with 2'-O-methyl-nucleotide substitutions [54,55] and the results showed that LC07 and LC09 still bound to K7M2 cells with high affinity but not to AML12 cells and PBMCs (Fig. 1c). In addition, LC07 and LC09 also bound to human OS cells (Saos-2) but not to human normal liver cells (THLE-3) and PBMCs (Supplementary Fig. 1a), implying their translational potentials in clinical application. Binding affinity of LC07 and LC09 with K7M2 cells, as quantified by equilibrium dissociation constants ( $K_d$ ) [36], was in the nanomolar-to-picomolar range (Fig. 1d). Finally, we chose LC09 for further studies due to its satisfactory secondary structure with lower predicted free energy and the least base number (Fig. 1e). We also evaluated the binding ability of LC09 with another mouse OS cells (K12), primary mouse osteoblasts and human breast cancer cells (MBA-MD-231), respectively. Results showed that LC09 aptamer recognized K12 cell rather than other cells, indicating the high specificity of the LC09 aptamer on OS cells (Supplementary Fig. 1b).

### 3.2. Selection of the optimal VEGFA gRNA for CRISPR/Cas9-based genome editing

6 candidate VEGFA gRNAs were chosen from GeCKOv2 libraries (Supplementary Table 2) [37]. To select the optimal gRNA, we constructed a series of CRISPR/Cas9 plasmids, which encoded different candidate gRNAs, Cas9 and the enhanced green fluorescent protein (EGFP) (Supplementary Fig. 2a). After transfection of these CRISPR/Cas9 plasmids into mouse OS cells (K7M2) by Lipofectamine 3000 at the same concentration, we detectable comparable Cas9 protein levels (Supplementary Fig. 2b) and EGFP fluorescence (Supplementary Fig. 2c). However, Surveyor assay showed that insertion/deletion (Indel) frequency of gRNA 2 was the highest among the 6 candidate gRNAs (Supplementary Fig. 2d). Levels of VEGFA in both lysates and supernatants of K7M2 cells transfected with CRISPR/Cas9 plasmids encoding gRNA 2 were the lowest, as determined by the enzyme-linked immunosorbent assay (ELISA) (Supplementary Fig. 2e). Sequencing analysis confirmed that gRNA 2 induced Indels at or near the cleavage site of VEGFA alleles and the lengths of the indels were mainly at 1 base pair (bp) or 2 bp, which lead to frame-shift mutation of VEGFA (>60%). (Supplementary Fig. 2f). We also predicted the off-target sites of gRNA 2 (Supplementary Table 3) and performed Surveyor assay. Results showed that there was no obvious Indel frequency for the off-target sites (Supplementary Fig. 2g). All the above results indicated that gRNA 2 was the optimal gRNA for CRISPR/Cas9-based VEGFA genome editing.

**Fig. 3. In vitro and ex vivo angiogenic activation by conditioned mediums from OS cells treated with different CRISPR/Cas9 formulations.** (a) Schematic diagram showing the experimental design. Briefly, mouse OS cells (K7M2) were cultured in medium with vehicle (PBS), PPC-CRISPR/Cas9, Rd-PPC-CRISPR/Cas9, LC09-PPC-CRISPR/Cas9 and LC09-PPC-CRISPR/Cas9 Ctrl, respectively. After 8 h, the medium was removed and the K7M2 cells were continuously incubated with fresh medium for another 48 h. Then, the conditioned medium was collected for culturing mouse primary endothelial cells. (b) The relative proliferation of endothelial cells incubated with the conditioned medium from K7M2 cells after treatment with vehicle (PBS) or different CRISPR/Cas9 formulations, as determined by CCK8 assay. The data are presented as the mean  $\pm$  sd; \* $P < 0.05$ . One-way ANOVA with a *post-hoc* test was performed and the statistical differences between the two groups were determined by the Student's *t*-test. (c) Wound healing assay to determine the migration of endothelial cells incubated with the conditioned medium from K7M2 cells after treatment with vehicle (PBS) or different CRISPR/Cas9 formulations. Scale bars, 400  $\mu$ m (d) Invasion of endothelial cells incubated with the conditioned medium from K7M2 cells after treatment with vehicle (PBS) or different CRISPR/Cas9 formulations, as determined by transwell invasion assay. Scale bars, 100  $\mu$ m. (e) Tube formation assay of primary endothelial cells incubated with the conditioned medium from K7M2 cells after treatment with vehicle (PBS) or different CRISPR/Cas9 formulations. Scale bars, 200  $\mu$ m. (f) Ex vivo aortic ring assay to determine vascular sprouting induced by the conditioned medium from K7M2 cells after treatment with vehicle (PBS) or different CRISPR/Cas9 formulations. Scale bars, 50  $\mu$ m.  $n = 6$  per group. The CRISPR/Cas9 plasmids encoded gRNA 2, while the CRISPR/Cas9 Ctrl plasmids encoded a non-sense gRNA. Rd, a random sequence served as a negative control of LC09 aptamer.

### 3.3. Preparation and in vitro characterization of LC09-PPC-CRISPR/Cas9

The preparation procedures for LC09 aptamer-functionalized CRISPR/Cas9 delivery system were shown in [Supplementary Fig. 3a](#). Briefly, CRISPR/Cas9 plasmids encoding gRNA 2, Cas9 and EGFP were spontaneously encapsulated in PPC lipopolymer. The 3' thiol- and 2'-O-methyl-modified LC09 was activated and conjugated to DSPE-PEG2000-Mal to form LC09-PEG2000-DSPE. Then, LC09-PEG2000-DSPE was inserted into the surface of PPC encapsulating CRISPR/Cas9 plasmids, *i.e.*, LC09-PPC-CRISPR/Cas9. Laser light scattering demonstrated that LC09-PPC-CRISPR/Cas9 had the diameter of  $163.1 \pm 17.2$  nm ([Supplementary Fig. 3b](#)) and the zeta potential of  $-12.7 \pm 2.1$  mV ([Supplementary Table 4](#)). The particle size of LC09-PPC-CRISPR/Cas9 was appropriate for passive tumor-targeting considering the more permeabilized blood vessels in tumor with the pore size ranging from 100 nm to 780 nm compared to the normal pore size <6 nm [56]. The encapsulation efficiency of the CRISPR/Cas9 was above 80% and the loading efficiency of LC09 was  $84.7 \pm 8.7\%$  for LC09-PPC-CRISPR/Cas9 ([Supplementary Table 4](#)). Representative image from cryogenic temperature transmission electron microscopy (cryo-TEM) showed the uniformity of particle distribution and a spherical shape ([Supplementary Fig. 3c](#)). Both 2'-O-methyl-modified LC09 aptamer and CRISPR/Cas9 plasmids encapsulated in PPC showed desirable serum stability at the examined time points, when compared to their respective free forms ([Supplementary Fig. 3d](#)), indicating the protection role of PPC for DNA plasmids from serum enzyme degradation.

### 3.4. In vitro cellular uptake, genome editing and anti-tumor activity

We labeled CRISPR/Cas9 plasmids with Cyanine 5 (Cy5) and investigated *in vitro* effects of LC09 aptamer on cellular uptake of the plasmids in OS cells (K7M2). A random sequence (Rd) served as the negative control for the LC09 aptamer. Flow cytometric analysis showed the most intense fluorescence signals in K7M2 cells treated with LC09-PPC-CRISPR/Cas9 when compared to PPC-CRISPR/Cas9, Rd-PPC-CRISPR/Cas9 and positive control Lipo 3000-CRISPR/Cas9 (Lipofectamine 3000-CRISPR/Cas9) ([Fig. 2a](#)). Then, we examined the expression and genome editing of different CRISPR/Cas9 formulations in K7M2 cells. Non-sense gRNA was used as a negative control for VEGFA gRNA 2. Significantly higher levels of Cas9 protein, EGFP fluorescence and Indel frequency as well as decreased VEGFA in both supernatants and lysates were observed in K7M2 cells treated with LC09-PPC-CRISPR/Cas9 when compared to other PPC-based CRISPR/Cas9 formulation groups or Lipo 3000-CRISPR/Cas9 ([Supplementary Fig. 4](#); [Fig. 2b](#) and c). In contrast to LC09-PPC-CRISPR/Cas9, we found no obvious decrease of VEGFA in both supernatants and lysates of K7M2 cells by LC09-PPC-CRISPR/Cas9 Ctrl, suggesting the specificity of the selected optimal gRNA 2 for VEGFA ([Fig. 2b](#) and c). To determine whether LC09 aptamer could facilitate VEGFA genome editing-mediated anti-tumor activity, we treated K7M2 cells with the CRISPR/Cas9 formulations and examined the cell viability, migration and invasion *in vitro* [43]. Our results showed that LC09-PPC-CRISPR/Cas9 dramatically inhibited viability, migration and invasion of K7M2 cells ([Fig. 2d–f](#)) than vehicle control (PBS) or other CRISPR/Cas9 formulations. The uptake, VEGFA gene editing and viability inhibition of LC09-PPC-CRISPR/Cas9 were confirmed in another mouse OS cell (K12) ([Supplementary Fig. 5](#)).

### 3.5. Mechanism of cellular uptake of LC09-PPC-CRISPR/Cas9

To investigate the cellular mechanism through which LC09-PPC-

CRISPR/Cas9 was taken up by OS cells, we labeled the CRISPR/Cas9 plasmids with Cy5 and treated OS cells (K7M2) with LC09-PPC-CRISPR/Cas9 in the presence of Alexa488-labeled endocytic marker including dextran (a marker of macropinocytosis), cholera toxin-B (a marker of caveolae-mediated endocytosis) and transferrin (a marker of clathrin-mediated endocytosis) [42], respectively. We observed numerous instances of co-localization of CRISPR/Cas9 plasmids with dextran and cholera toxin-B, but not with transferrin by confocal microscopy ([Supplementary Fig. 6a](#)), indicating that LC09-PPC-CRISPR/Cas9 could be taken up via macropinocytosis and caveolae-mediated endocytosis. Further, blockage of either macropinocytosis or caveolae-mediated endocytosis by their respective chemical inhibitors reduced the fluorescence signals of Cy5-labeled CRISPR/Cas9 plasmids in K7M2 cells treated with LC09-PPC-CRISPR/Cas9 in a dose-dependent manner ([Supplementary Fig. 6b](#)). Notably, reduction of the fluorescence signals by inhibitors of macropinocytosis was more remarkable than that by inhibitors of caveolae-mediated endocytosis, indicating that macropinocytosis was mainly responsible for cellular uptake of LC09-PPC-CRISPR/Cas9. Macropinocytosis is an endocytosis pathway that permits bulk uptake [57], which possibly led to efficient internalization of LC09-PPC-CRISPR/Cas9 ([Supplementary Fig. 6b](#)).

### 3.6. In vitro and ex vivo angiogenic activation by conditioned medium from OS cells

OS cells (K7M2) were treated with different CRISPR/Cas9 formulations and the conditioned medium was collected. We incubated the mouse primary endothelial cells with the conditioned media to determine their *in vitro* angiogenic activity, including proliferation, migration, invasion and tube formation of endothelial cells [47,58] ([Fig. 3a](#)). Compared to conditioned medium from K7M2 cells after treatment with vehicle (PBS), PPC-CRISPR/Cas9, Rd-PPC-CRISPR/Cas9 or LC09-PPC-CRISPR/Cas9 Ctrl, we observed weaker proliferation, migration, invasion and tube formation of endothelial cells incubated with conditioned medium from K7M2 cells after treatment with LC09-PPC-CRISPR/Cas9 ([Fig. 3b–e](#)). In addition, reduced proliferation and tube formation of endothelial cells treated with conditioned medium from another OS cell line K12 after treatment with LC09-PPC-CRISPR/Cas9 were also observed ([Supplementary Fig. 7](#)). In addition, we performed *ex vivo* aortic ring assay [59,60] to examine angiogenic effects of the conditioned medium. Conditioned medium from K7M2 cells treatment with LC09-PPC-CRISPR/Cas9 induced less vascular sprouting of the aortic ring than conditioned medium from K7M2 cells treated with vehicle (PBS) or other CRISPR/Cas9 formulations ([Fig. 3f](#)).

### 3.7. In vivo tissue distribution and tumor cell-specific delivery

We established a syngeneic orthotopic OS mouse model with spontaneous lung metastasis by intraosseous inoculation of OS cells (K7M2) [48]. *In vivo* tissue distribution of Cy5-labeled CRISPR/Cas9 plasmids delivered by different carriers in tumor and major organs were quantified by evaluating the percentage of injected dose in those tissues at various time points after the intravenous administration [61,62]. The results showed low accumulations of CRISPR/Cas9 in the heart, spleen, kidney and paracancerous tissue in lung in all administration groups ([Fig. 4a](#)). The accumulations of LC09-PPC-CRISPR/Cas9 were significantly stronger in orthotopic OS tissues and metastatic OS tissues in lung however considerably lower in liver and other organs when compared to PPC-CRISPR/Cas9 or Rd-PPC-CRISPR/Cas9 ( $P < 0.05$ ) at all the time points ([Fig. 4a](#)). LC09-PPC-CRISPR/Cas9 achieved the highest concentration in both orthotopic and metastatic OS tissues at 4 h ([Fig. 4a](#)). The tissue

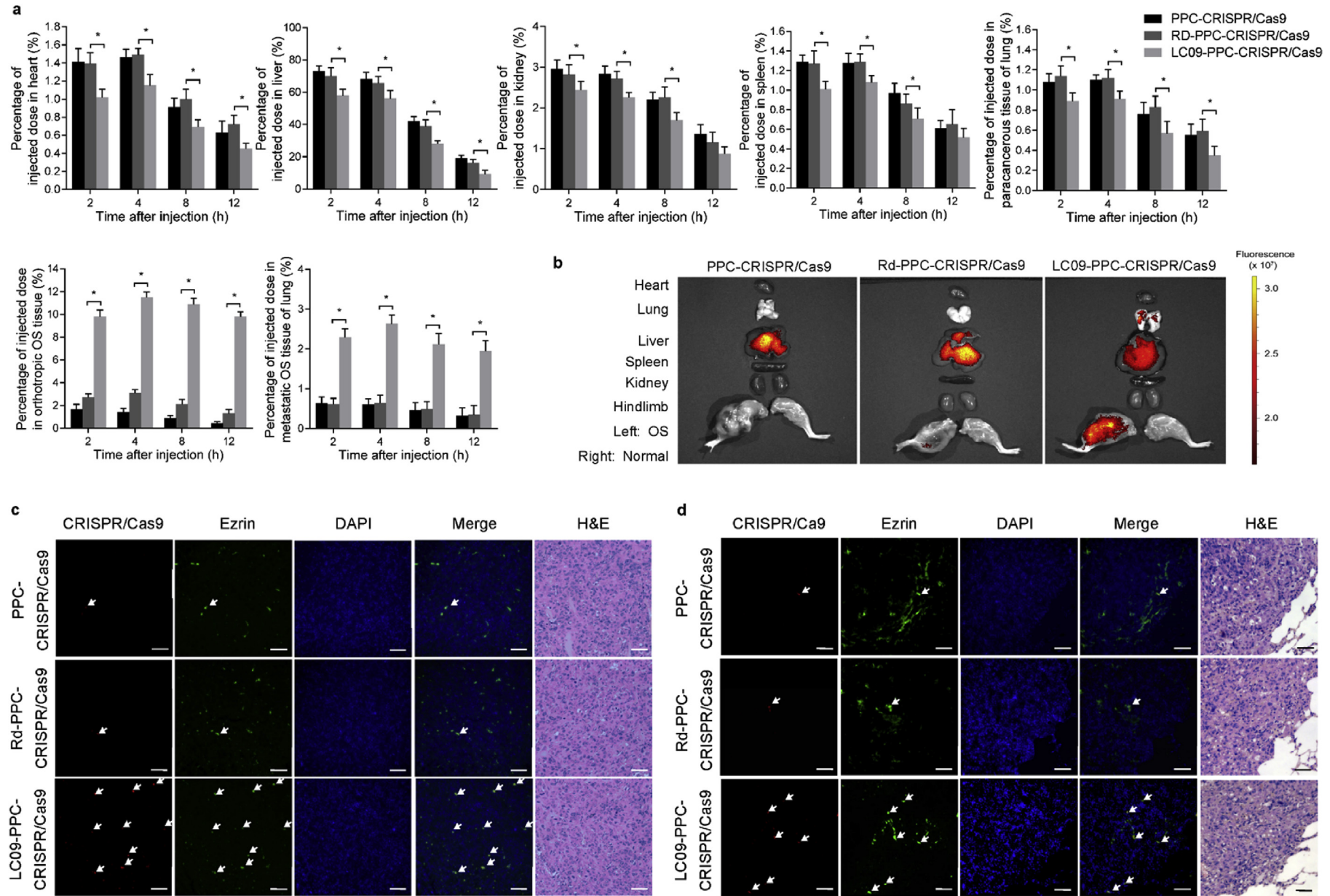


**Fig. 4. In vivo tissue distribution and tumor cell-specific delivery of different CRISPR/Cas9 formulations.** (a) Quantitative analysis of Cy5-labeled CRISPR/Cas9 plasmids in major organs (heart, liver, kidney, spleen, orthotropic OS tissue, metastatic OS tissue of lung and paracancerous tissue of lung) from syngeneic orthotropic OS mice intravenously administered with PPC-CRISPR/Cas9, Rd-PPC-CRISPR/Cas9 or LC09-PPC-CRISPR/Cas9, respectively. \*P < 0.05 vs. PPC-CRISPR/Cas9 or Rd-PPC-CRISPR/Cas9. (b) Localization of Cy5-labeled CRISPR/Cas9 plasmids in major organs (heart, liver, kidney, spleen, OS-bearing hindlimb, lung with tumor metastasis and normal hindlimb) from syngeneic orthotropic OS mice intravenously administered with PPC-CRISPR/Cas9, Rd-PPC-CRISPR/Cas9 or LC09-PPC-CRISPR/Cas9, visualized by biophotonic imaging. Yellow, highest fluorescence intensity. (c, d) Fluorescence micrographs of OS tissues (c) and lung metastatic sites (d) from mice administrated with PPC-CRISPR/Cas9 (top row), Rd-PPC-CRISPR/Cas9 (middle row) or LC09-PPC-CRISPR/Cas9 (bottom row). The CRISPR/Cas9 plasmids were labeled with Cy5 (red; left column). Immunofluorescence staining was performed to detect Ezrin-positive tumor cells (green; middle left column). Merged images with DAPI staining showed co-localization of CRISPR/Cas9 plasmids with Ezrin-positive tumor cells (arrows and yellow color, middle right column). H&E staining of the adjacent sections was included at right. Scale bars, 50  $\mu$ m. n = 6 per group. Rd, a random sequence served as a negative control of LC09 aptamer.

distribution was then further confirmed by biophotonic imaging, and the fluorescence signals observed in orthotopic OS and major organs collected from different groups at 4 h after administration were consistent with the percentage of dose results (Fig. 4b). To investigate whether LC09 could facilitate the delivery of CRISPR/Cas9 plasmids into tumor cells, we examined the co-localization of Cy5-labeled CRISPR/Cas9 plasmids with OS markers (Ezrin) [63] in cytosections of orthotopic OS tissues and lung metastatic sites from mice administrated with different CRISPR/Cas9 formulations. We found numerous instances of co-localization of Cy5-labeled CRISPR/Cas9 plasmids in OS tissues and lung metastatic sites from mice when LC09-PPC-CRISPR/Cas9 was administered, whereas there were few instances of such overlapping staining in OS tissues and lung metastatic sites from mice administrated with PPC-CRISPR/Cas9 or Rd-PPC-CRISPR/Cas9 (Fig. 4c and d). This suggested that LC09 could deliver PPC encapsulated CRISPR/Cas9 into OS cells in regardless of the location (orthotopic tumor or metastatic sites).

### 3.8. In vivo tumor-specific expression of CRISPR/Cas9

We examined *in vivo* tumor-specific expression of CRISPR/Cas9 plasmids in syngeneic orthotopic OS mice over time after intravenous administration of different CRISPR/Cas9 formulations by CRISPR/Cas9 ELISA kit. Since the second day after administration, Cas9 expressions of LC09-PPC-CRISPR/Cas9 group in both orthotopic and metastatic OS tissues were significantly higher when compared to those of PPC-CRISPR/Cas9 or Rd-PPC-CRISPR/Cas9 group ( $P < 0.05$ ) (Supplementary Fig. 8a). The levels of Cas9 of both OS tissues in LC09-PPC-CRISPR/Cas9 group reached the peak at 8 d, dropped half at 14 d, and maintained significant until 17 d. This suggested that 14 days (two weeks) would be suitable for the dosing interval of the *in vivo* treatment by LC09-PPC-CRISPR/Cas9 (Supplementary Fig. 8a). In addition, EGFP encoded by CRISPR/Cas9 plasmids, used as an indicator for expression of CRISPR/Cas9, was analyzed by biophotonic imaging at 14 d. As shown in biophotonic images, fluorescence signals of LC09-PPC-CRISPR/Cas9 were more noticeable in OS-bearing hindlimb and lung with tumor metastasis but lower in liver when compared to PPC-CRISPR/Cas9 or Rd-PPC-CRISPR/Cas9 (Supplementary Fig. 8b). We found no detectable fluorescence in the heart, spleen and kidney in all administration groups (Supplementary Fig. 8b). The Cas9 expressions in OS tissues, lung metastasis and liver tissues examined by western blotting were consistent with biophotonic results (Supplementary Fig. 8c).

### 3.9. In vivo genome editing, anti-tumor activity and anti-metastasis

Mice were intraosseous inoculated with OS cells (K7M2) and left untreated for three weeks. According to the Cas9 expression curve in Supplementary Fig. 8a, we administered three periodic intravenous injections of CRISPR/Cas9 plasmids ( $0.75 \text{ mg kg}^{-1}$ ) encapsulated in different carriers to syngeneic orthotopic OS mice at an interval of two weeks (Supplementary Fig. 9a). LC09-PPC-CRISPR/Cas9 induced significantly higher Indels in OS tissues and lung metastatic sites however considerable less Indels in liver tissues compared to vehicle (PBS), PPC-CRISPR/Cas9, Rd-PPC-CRISPR/Cas9 or LC09-PPC-CRISPR/Cas9 Ctrl (Supplementary Fig. 9b). Moreover, reduced expression of VEGFA in OS tissues and lung metastatic sites were detected for LC09-PPC-CRISPR/Cas9 treated mice (Supplementary Fig. 9c). Immunohistochemical analysis showed the lower levels of VEGFA, Ki67 (a marker of proliferation) [64], Ezrin (a marker of metastasis) [65], MMP9 (a marker of invasion) [66] and Survivin (a marker of anti-apoptosis) [67] in OS tissues from mice administered with LC09-PPC-CRISPR/Cas9 when compared to vehicle (PBS), PPC-CRISPR/Cas9, Rd-PPC-CRISPR/Cas9

or LC09-PPC-CRISPR/Cas9 Ctrl (Fig. 5a). Size and volume of OS tissue were smaller in LC09-PPC-CRISPR/Cas9-treated mice than other treatment groups (Fig. 5b and c). Furthermore, LC09-PPC-CRISPR/Cas9, rather than vehicle (PBS) and other CRISPR/Cas9 formulations, decreased expression of VEGFA and markers of proliferation, metastasis, invasion and anti-apoptosis in lung metastatic sites (Fig. 6a) as well as numbers of lung metastatic sites (Fig. 6b and c).

### 3.10. In vivo inhibition of angiogenesis and bone destruction and toxicity

We also evaluated *in vivo* angiogenesis by Matrigel plug assay [51] and immunohistochemistry and bone destruction by microCT in OS tissues from syngeneic orthotopic OS mice with periodic intravenous injections of CRISPR/Cas9 plasmids ( $0.75 \text{ mg kg}^{-1}$ ) encapsulated in different carriers. Compared to mice administered with vehicle (PBS), PPC-CRISPR/Cas9, Rd-PPC-CRISPR/Cas9 or LC09-PPC-CRISPR/Cas9 Ctrl, mice treated with LC09-PPC-CRISPR/Cas9 exhibited less neovascularization in subcutaneously implanted Matrigel in OS region (Fig. 7a), decreased expression of endothelial cell activation markers including CD34 and von Willebrand Factor (vWF) [68] (Fig. 7b) and relieved bone destruction in OS tissues (Fig. 7c). To determine the toxicity of LC09-PPC-CRISPR/Cas9, we performed biochemical and hematological assays in syngeneic orthotopic OS mice after single or multiple injection(s) of LC09-PPC-CRISPR/Cas9. There was no significant change of biochemical parameters including liver function indexes (alanine aminotransferase (ALT) and aspartate aminotransferase (AST)) and a kidney function index (blood urea nitrogen (BUN)), as well as hematologic parameters, such as hematocrit (HCT), red blood cell (RBC), haemoglobin (HGB), white blood cell (WBC) and platelet (PLT), between LC09-PPC-CRISPR/Cas9 groups and vehicle (PBS) group (Supplementary Table 5).

## 4. Discussion

Our work demonstrated an LC09 aptamer-functionalized *in vivo* CRISPR/Cas9 delivery system, which facilitated distribution of CRISPR/Cas9 in both orthotopic OS and lung metastasis, resulting in tumor cell-selective VEGFA disruption and inhibition of OS malignancy, lung metastasis, angiogenesis as well as bone destruction with no detectable toxicity.

In tumor biology and therapy, an important advance is the discovery of autocrine and paracrine VEGF signaling in tumor cells, which contributes to angiogenesis and tumorigenesis [10,69]. Therapeutic strategies targeting VEGF signaling have been developed for tumor treatment [69]. A recombinant humanized anti-VEGF monoclonal antibody (Bevacizumab) alone or in combination with chemotherapeutics has been approved or under clinical trials for ovarian cancer, metastatic breast cancer, non-small-cell lung cancer, OS and other cancers [70,71]. However, Bevacizumab also blocks VEGF action in normal organs after systemic use and causes adverse effects such as hypertension, proteinuria and upper respiratory infection [72]. In our study, we found that LC09 facilitated CRISPR/Cas9-mediated disruption of both autocrine (evidenced by anti-tumor activity of LC09-CRISPR/Cas9 *in vitro*) and paracrine VEGFA signaling (suggested by anti-endothelial cell activation by conditioned medium from OS cells treated with LC09-CRISPR/Cas9 *in vitro*) in OS cells and tumor-selective distribution of CRISPR/Cas9, leading to satisfactory therapeutic effects in syngeneic orthotopic OS mice.

Clinical implementation of CRISPR/Cas9 technology in cancer therapy requires safe and effective tumor-targeted *in vivo* delivery systems. Recently, a study proposed an artificial CRISPR/Cas9 virus with a RGD-R8-PEG-HA shell for treating ovarian cancer. The

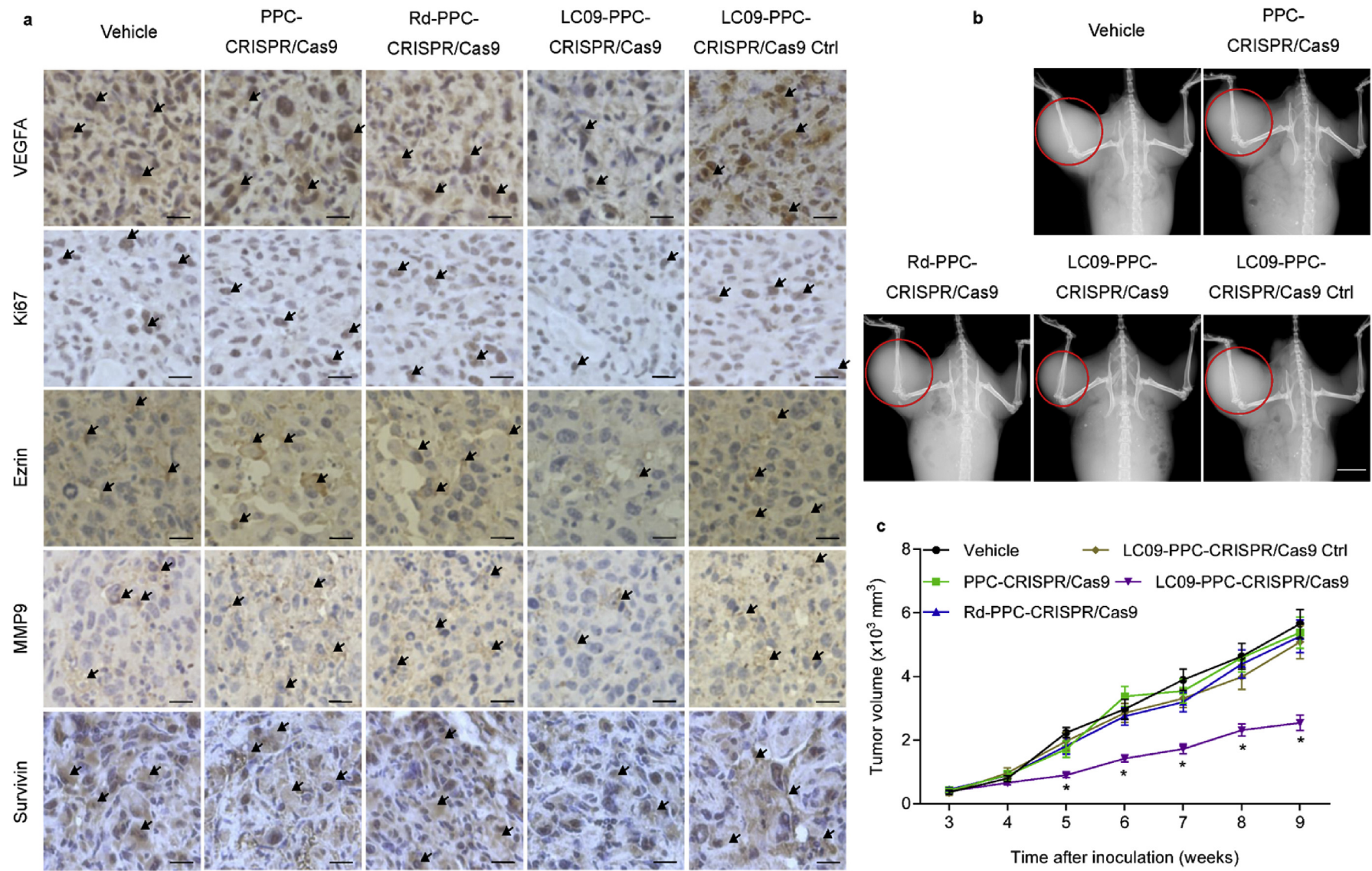


**Fig. 5. In vivo anti-tumor activity of CRISPR/Cas9 delivered by different carriers in OS tissues.** (a) Immunohistochemical detection of VEGFA, Ki67 (a marker of proliferation), Ezrin (a marker of metastasis), MMP9 (a marker of invasion) and Survivin (a marker of anti-apoptosis) in paraffin-embedded OS tissues from syngeneic orthotopic OS mice administrated with vehicle (PBS), PPC-SRISPR-Cas9, Rd-PPC-SRISPR-Cas9, LC09-PPC-SRISPR-Cas9 and LC09-PPC-SRISPR-Cas9 Ctrl, respectively. Black arrows indicated positive staining by the corresponding antibodies. Scale bars, 20  $\mu\text{m}$ . (b) Representative X-ray images showing the size of OS tissues from syngeneic orthotopic OS mice administrated with vehicles (PBS) or CRISPR/Cas9 delivered by different carriers. Red circles indicated the OS tissue on hindlimb. Scale bars, 1 cm. (c) Volume of OS tissues from syngeneic orthotopic OS mice administrated with vehicles (PBS) or different CRISPR/Cas9 formulations at different time points, calculated by the formula: volume = (width) $^2$  x length/2, with subtraction of normal tissue volume of the contralateral non-tumor hindlimb. The data are presented as the mean  $\pm$  sd; \* $P < 0.05$ . One-way ANOVA with a post-hoc test was performed and the statistical differences between the two groups were determined by the Student's t-test.  $n = 9$  per group. The CRISPR/Cas9 plasmids encoded gRNA 2, while the CRISPR/Cas9 Ctrl plasmids encoded a non-sense gRNA. Rd, a random sequence served as a negative control of LC09 aptamer.

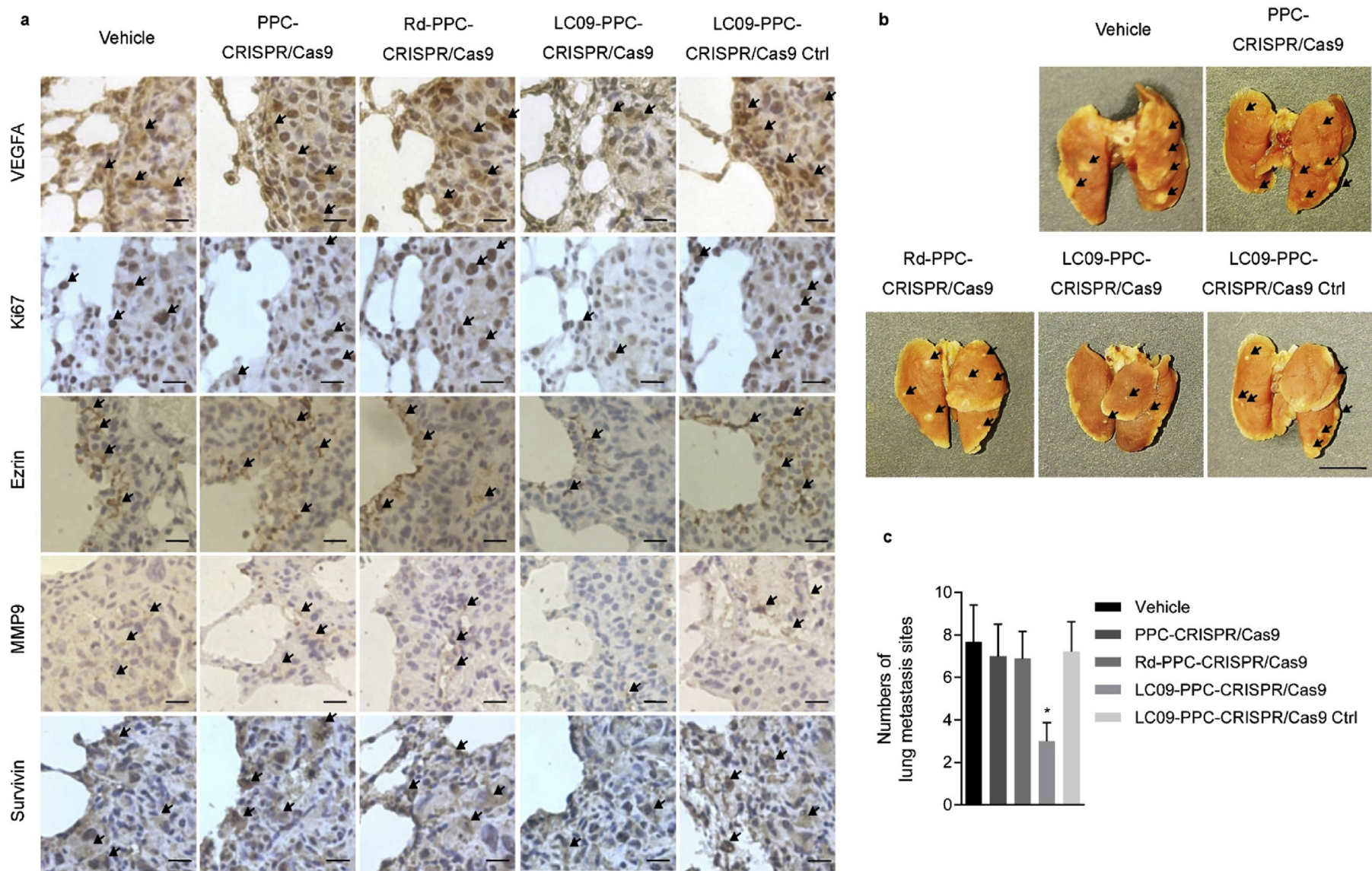


**Fig. 6. In vivo anti-metastasis of different CRISPR/Cas9 formulations.** (a) Immunohistochemical staining of VEGFA, Ki67 (a marker of proliferation), Ezrin (a marker of metastasis), MMP9 (a marker of invasion) and Survivin (a marker of anti-apoptosis) in lung metastatic sites from syngeneic orthotopic OS mice administrated with vehicle (PBS), PPC-SRISPR-Cas9, Rd-PPC-SRISPR-Cas9, LC09-PPC-SRISPR-Cas9 and LC09-PPC-SRISPR-Cas9 Ctrl, respectively. Black arrows indicated positive staining by the corresponding antibodies. Scale bars, 20  $\mu$ m. (b) Representative images showing lung with metastatic sites in syngeneic orthotopic OS mice administrated with vehicle (PBS) or CRISPR/Cas9 delivered by different carriers. Black arrows indicated tumor metastatic sites. Scale bar, 500 mm. (c) Number of metastatic sites on lung from syngeneic orthotopic OS mice administrated with vehicles (PBS) or different CRISPR/Cas9 formulations. The data are presented as the mean  $\pm$  sd; \*P < 0.05. One-way ANOVA with a post-hoc test was performed and the statistical differences between the two groups were determined by the Student's t-test. n = 9 per group. The CRISPR/Cas9 plasmids encoded gRNA 2, while the CRISPR/Cas9 Ctrl plasmids encoded a non-sense gRNA. Rd, a random sequence served as a negative control of LC09 aptamer.

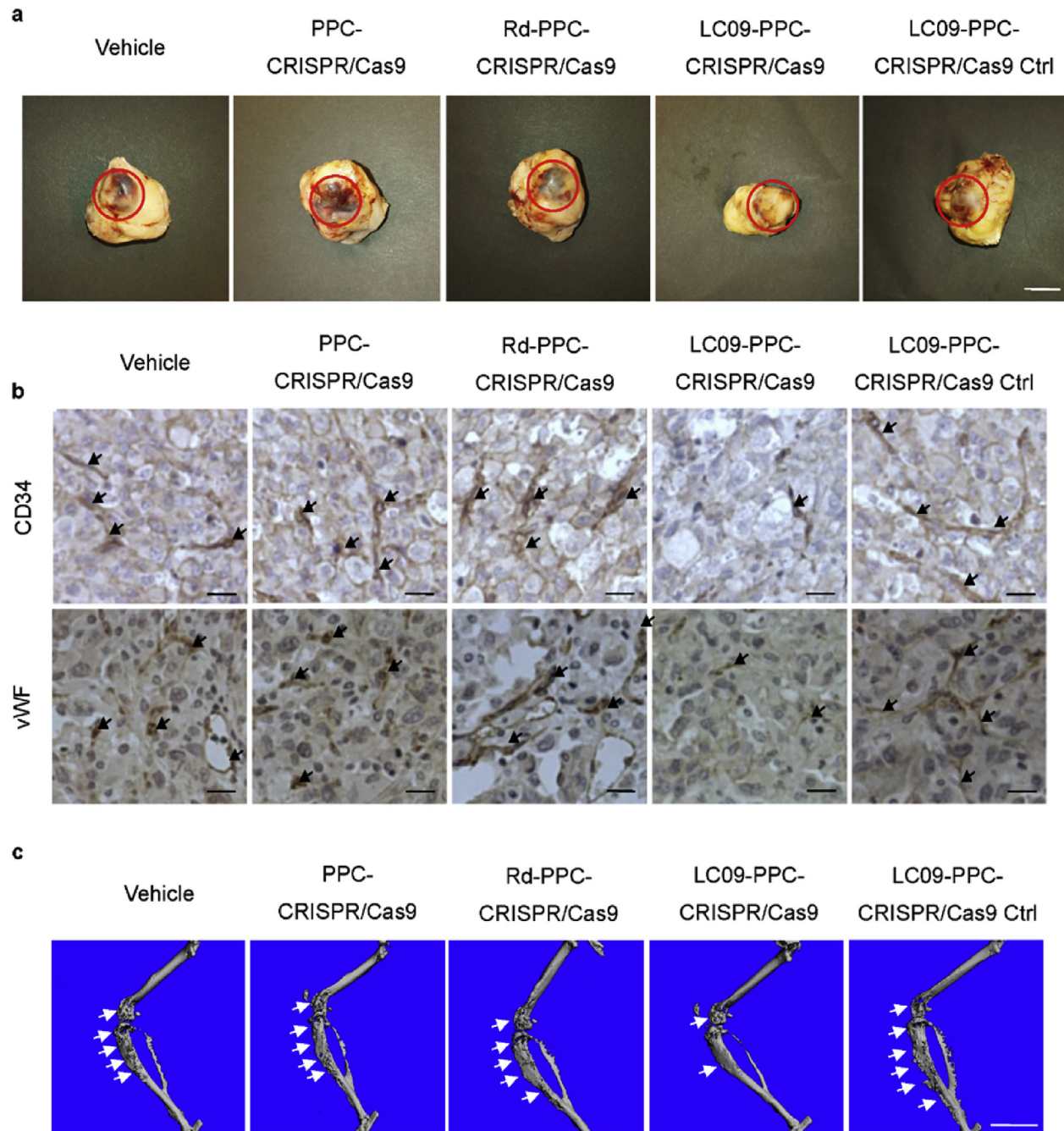


**Fig. 7. In vivo anti-angiogenesis and anti-bone destruction of different CRISPR/Cas9 formulations in OS tissues.** (a) Matrigel plug assay showing in vivo neovascularization around OS tissues from syngeneic orthotopic OS mice administrated with vehicle (PBS), PPC-CRISPR-Cas9, Rd-PPC-CRISPR-Cas9, LC09-PPC-CRISPR-Cas9 and LC09-PPC-CRISPR-Cas9 Ctrl, respectively. 200  $\mu$ l Matrigel was subcutaneously injected in OS region 10 d before the mice were euthanized. Red circles indicated representative Matrigel plugs. Scale bars, 1 cm. (b) Immunohistochemical detection of angiogenesis using anti-von Willebrand Factor (vWF) and CD34 antibodies in paraffin-embedded OS tissues from mice intravenously administered with vehicles (PBS) or different CRISPR/Cas9 formulations. Scale bars, 20  $\mu$ m. (c) microCT analysis to examine bone lesion of tibiae from mice intravenously administered with vehicles (PBS) or different CRISPR/Cas9 formulations. White arrows indicated bone destruction sites. Scale bars, 5 mm.  $n = 9$  per group. The CRISPR/Cas9 plasmids encoded gRNA 2, while the CRISPR/Cas9 Ctrl plasmids encoded a non-sense gRNA. Rd, a random sequence served as a negative control of LC09 aptamer.

hyaluronic acid (HA) binding to the CD44 receptors was designed as the tumor recognition element [73]. Nevertheless, CD44 is also highly expressed in immune cells [74] and a potential concern regarding the targeting specificity still exists. Here, we screened the LC09 aptamer specifically targeting both human and mouse OS cells. *In vitro* data showed that LC09 has no binding ability to hepatocytes and PBMCs. Consistently, *in vivo* data demonstrated that

LC09 facilitated tumor cell-selective distribution and expression of CRISPR/Cas9 in both orthotopic OS and lung metastasis and minimized liver accumulation of CRISPR/Cas9.

Safety issue is one of the major hurdles to the clinical translation of CRISPR-Cas9 technology [75]. Previously, adeno-associated virus (AAV)-assisted delivery of the CRISPR/Cas9 has shown gene silencing efficacy *in vivo* [76]. However, the long persistence and

immunogenicity in the host prevent the wide therapeutic application of AAV-based CRISPR/Cas9 delivery [22,73]. Recently, different carriers of CRISPR/Cas9 including combined lipid nanoparticle and AAV, artificial virus and non-viral nanoparticles has been developed [22,36,77]. In our work, we used the PPC lipopolymer, a well-tolerated non-virus plasmid carrier under clinical trials [78], as the packaging carriers of CRISPR/Cas9. Furthermore, aptamer with no immunogenicity [54] was linked on the surface of PPC. CRISPR/Cas9 plasmids encoding the optimal gRNA 2 with no obvious off-target effects were encapsulated in PPC. As expected, our data showed no significant toxicity of LC09-PPC-CRISPR/Cas9 after *in vivo* systemic administration.

## 5. Conclusions

In summary, the OS cell-specific aptamer (LC09) we screened facilitated selective distribution of CRISPR/Cas9 in both orthotopic OS tissue and metastatic OS tissue of lung lesion, leading to effective VEGFA genome editing in tumor, decreased VEGFA expression and secretion, inhibited orthotopic OS malignancy and lung metastasis, as well as reduced angiogenesis and bone lesion with no detectable toxicity. The aptamer-functionalized PPC lipopolymer could be a promising *in vivo* tumor-targeted delivery system for therapeutic CRISPR/Cas9. This work may pave the road for new clinical approaches using CRISPR/Cas9 in cancer treatment.

## Competing interests statements

The authors declare that they have no competing financial interests.

## Acknowledgements

We thank the technical staff (Ms. Yeuk Siu Cheung and Mr. Chi Leung Chan) from Law Sau Fai Institute for Advancing Translational Medicine in Bone and Joint Diseases, Hong Kong Baptist University for providing critical comments and technical support. This study was supported by the Ministry of Science and Technology of China (2013ZX09301307 to A.L.), the Hong Kong General Research Fund (HKBU479111 to G.Z., HKBU478312 to G.Z., HKBU262913 to G.Z., HKBU12102914 to G.Z., HKBU261113 to A.L. HKBU212111 to H.Z., HKBU212613 to H.Z., CUHK14112915 to B.Z. and CUHK489213 to B.Z.), the Natural Science Foundation Council of China (81272045 to G.Z., 81703049 to F.L., 81272045 to B.G., 81401833 to B.G. and 81470072 to X.H.), the Research Grants Council and Natural Science Foundation Council of China (N\_HKBU435/12 to G.Z.), the Croucher Foundation (Gnt#CAS14BU/CAS14201 to G.Z.), the Interdisciplinary Research Matching Scheme (IRMS) of Hong Kong Baptist University (RC-IRMS/12-13/02 to A.L., RC-IRMS/13-14/02 to G.Z. and RC-IRMS/15-16/01 to A.L.), the Hong Kong Baptist University Strategic Development Fund (SDF13-1209-P01 to A.L.), the Hong Kong Research Grants Council Early Career Scheme (489213 to G.Z.), the Inter-institutional Collaborative Research Scheme of Hong Kong Baptist University (RC-ICRS/14-15/01 to G.Z.), the Faculty Research Grant of Hong Kong Baptist University (FRG1/13-14/024 to G.Z., FRG2/13-14/006 to G.Z., FRG2/14-15/010 to G.Z. and FRG2/14-15/063 to H.Z.), the China Academy of Chinese Medical Sciences (Z0252 and Z0293 to A.L.), Science and Technology Innovation Commission of Shenzhen Municipality Funds (JCYJ20170307161659648 to F. L.).

## Appendix A. Supplementary data

Supplementary data related to this article can be found at <http://dx.doi.org/10.1016/j.biomaterials.2017.09.015>.

## References

- [1] J. Gill, M.K. Ahluwalia, D. Geller, R. Gorlick, New targets and approaches in osteosarcoma, *Pharmacol. Ther.* 137 (2013) 89–99.
- [2] S.M. Botter, D. Neri, B. Fuchs, Recent advances in osteosarcoma, *Curr. Opin. Pharmacol.* 16 (2014) 15–23.
- [3] D. Saha, K. Saha, A. Banerjee, D. Jash, Osteosarcoma relapse as pleural metastasis, *South Asian J. Cancer* 2 (2013) 56.
- [4] Z.S. Kundu, Classification, imaging, biopsy and staging of osteosarcoma, *Indian J. Orthop.* 48 (2014) 238–246.
- [5] A.P. Staddon, R. Lackman, K. Robinson, J.B. Shrager, M. Warhol, Osteogenic sarcoma presenting with lung metastasis, *Oncologist* 7 (2002) 144–153.
- [6] M. Kansara, M.W. Teng, M.J. Smyth, D.M. Thomas, Translational biology of osteosarcoma, *Nat. Rev. Cancer* 14 (2014) 722–735.
- [7] M.P. Link, A.M. Goorin, A.W. Miser, A.A. Green, C.B. Pratt, J.B. Belasco, et al., The effect of adjuvant chemotherapy on relapse-free survival in patients with osteosarcoma of the extremity, *N. Engl. J. Med.* 314 (1986) 1600–1606.
- [8] P.A. Meyers, J.H. Healey, A.J. Chou, L.H. Wexler, P.R. Merola, C.D. Morris, et al., Addition of pamidronate to chemotherapy for the treatment of osteosarcoma, *Cancer* 117 (2011) 1736–1744.
- [9] A. Hoeben, B. Landuyt, M.S. Highley, H. Wildiers, A.T. Van Oosterom, E.A. De Brujin, Vascular endothelial growth factor and angiogenesis, *Pharmacol. Rev.* 56 (2004) 549–580.
- [10] H.L. Goel, A.M. Mercurio, VEGF targets the tumour cell, *Nat. Rev. Cancer* 13 (2013) 871–882.
- [11] M. Nguyen, Angiogenic factors as tumor markers, *Investig. New Drugs* 15 (1997) 29–37.
- [12] G. Niu, X. Chen, Vascular endothelial growth factor as an anti-angiogenic target for cancer therapy, *Curr. Drug Targets* 11 (2010) 1000–1017.
- [13] J. Yang, D. Yang, Y. Sun, B. Sun, G. Wang, J.C. Trent, et al., Genetic amplification of the vascular endothelial growth factor (VEGF) pathway genes, including VEGFA, in human osteosarcoma, *Cancer* 117 (2011) 4925–4938.
- [14] T. Tanaka, Y. Yui, N. Naka, T. Wakamatsu, K. Yoshioka, N. Araki, et al., Dynamic analysis of lung metastasis by mouse osteosarcoma LM8: VEGF is a candidate for anti-metastasis therapy, *Clin. Exp. Metastasis* 30 (2013) 369–379.
- [15] P.G. Daft, Y. Yang, D. Napierala, M. Zayzafoon, The growth and aggressive behavior of human osteosarcoma is regulated by a CaMKII-controlled autocrine VEGF signaling mechanism, *PLoS One* 10 (2015), e0121568.
- [16] J. Zhao, Z.R. Zhang, N. Zhao, B.A. Ma, Q.Y. Fan, VEGF silencing inhibits human osteosarcoma angiogenesis and promotes cell apoptosis via PI3K/AKT signaling pathway, *Int. J. Clin. Exp. Med.* 8 (2015) 12411–12417.
- [17] N. Savic, G. Schwank, Advances in therapeutic CRISPR/Cas9 genome editing, *Transl. Res. J. Lab. Clin. Med.* 168 (2016) 15–21.
- [18] P.D. Hsu, E.S. Lander, F. Zhang, Development and applications of CRISPR-Cas9 for genome engineering, *Cell* 157 (2014) 1262–1278.
- [19] J. Shi, E. Wang, J.P. Milazzo, Z. Wang, J.B. Kinney, C.R. Vakoc, Discovery of cancer drug targets by CRISPR-Cas9 screening of protein domains, *Nat. Biotechnol.* 33 (2015) 661–667.
- [20] B.P. Kleinstiver, M.S. Prew, S.Q. Tsai, V.V. Topkar, N.T. Nguyen, Z. Zheng, et al., Engineered CRISPR-Cas9 nucleases with altered PAM specificities, *Nature* 523 (2015) 481–485.
- [21] Y. Nihongaki, F. Kawano, T. Nakajima, M. Sato, Photoactivatable CRISPR-Cas9 for optogenetic genome editing, *Nat. Biotechnol.* 33 (2015) 755–760.
- [22] C. Jiang, M. Mei, B. Li, X. Zhu, W. Zu, Y. Tian, et al., A non-viral CRISPR/Cas9 delivery system for therapeutic gene targeting *in vivo*, *Cell Res.* 27 (2017) 440–443.
- [23] J. Zhou, J.J. Rossi, Cell-specific aptamer-mediated targeted drug delivery, *Oligonucleotides* 21 (2011) 1–10.
- [24] Y. Zhang, H. Hong, W. Cai, Tumor-targeted drug delivery with aptamers, *Curr. Med. Chem.* 18 (2011) 4185–4194.
- [25] J.G. Fewell, M. Matar, G. Slobodkin, S.O. Han, J. Rice, B. Hovanes, et al., Synthesis and application of a non-viral gene delivery system for immunogene therapy of cancer, *J. Control. Release Off. J. Control. Release Soc.* 109 (2005) 288–298.
- [26] D.A. Wang, A.S. Narang, M. Kotb, A.O. Gaber, D.D. Miller, S.W. Kim, et al., Novel branched poly(ethylenimine)-cholesterol water-soluble lipopolymers for gene delivery, *Biomacromolecules* 3 (2002) 1197–1207.
- [27] D.Y. Furgeson, R.N. Cohen, R.I. Mahato, S.W. Kim, Novel water insoluble lipoparticulates for gene delivery, *Pharm. Res.* 19 (2002) 382–390.
- [28] R.D. Alvarez, M.W. Sill, S.A. Davidson, C.Y. Muller, D.P. Bender, R.L. DeBernardo, et al., A phase II trial of intraperitoneal EGEN-001, an IL-12 plasmid formulated with PEG-PEI-cholesterol lipopolymer in the treatment of persistent or recurrent epithelial ovarian, fallopian tube or primary peritoneal cancer: a gynecologic oncology group study, *Gynecol. Oncol.* 133 (2014) 433–438.
- [29] H. Yin, R.L. Kanasty, A.A. Eltoukhy, A.J. Vegas, J.R. Dorkin, D.G. Anderson, Non-viral vectors for gene-based therapy, *Nat. Rev. Genet.* 15 (2014) 541–555.
- [30] K. Di Gregoli, N. Jenkins, R. Salter, S. White, A.C. Newby, J.L. Johnson, Micro-RNA-24 regulates macrophage behavior and retards atherosclerosis, *Arterioscler. Thromb. Vasc. Biol.* 34 (2014) 1990–2000.
- [31] M. Giannotta, M. Trani, E. Dejana, VE-cadherin and endothelial adherens junctions: active guardians of vascular integrity, *Dev. Cell* 26 (2013) 441–454.
- [32] M. Miettinen, A.E. Lindenmayer, A. Chaubal, Endothelial cell markers CD31, CD34, and BNH9 antibody to H- and Y-antigens—evaluation of their specificity

- and sensitivity in the diagnosis of vascular tumors and comparison with von Willebrand factor, *Mod. Pathol. Off. J. U. S. Can. Acad. Pathol. Inc* 7 (1994) 82–90.
- [33] X. Cao, S. Li, L. Chen, H. Ding, H. Xu, Y. Huang, et al., Combining use of a panel of ssDNA aptamers in the detection of *Staphylococcus aureus*, *Nucleic Acids Res.* 37 (2009) 4621–4628.
- [34] S. Li, H. Xu, H. Ding, Y. Huang, X. Cao, G. Yang, et al., Identification of an aptamer targeting hnRNP A1 by tissue slide-based SELEX, *J. Pathol.* 218 (2009) 327–336.
- [35] K. Sefah, D. Shangguan, X. Xiong, M.B. O'Donoghue, W. Tan, Development of DNA aptamers using Cell-SELEX, *Nat. Protoc.* 5 (2010) 1169–1185.
- [36] C. Liang, B. Guo, H. Wu, N. Shao, D. Li, J. Liu, et al., Aptamer-functionalized lipid nanoparticles targeting osteoblasts as a novel RNA interference-based bone anabolic strategy, *Nat. Med.* 21 (2015) 288–294.
- [37] N.E. Sanjana, O. Shalem, F. Zhang, Improved vectors and genome-wide libraries for CRISPR screening, *Nat. Methods* 11 (2014) 783–784.
- [38] I.E. Lawhorn, J.P. Ferreira, C.L. Wang, Evaluation of sgRNA target sites for CRISPR-mediated repression of TP53, *PLoS One* 9 (2014), e113232.
- [39] F.A. Ran, P.D. Hsu, J. Wright, V. Agarwala, D.A. Scott, F. Zhang, Genome engineering using the CRISPR-Cas9 system, *Nat. Protoc.* 8 (2013) 2281–2308.
- [40] D. Patrick, D.A.S. Hsu, Joshua A. Weinstein, F. Ann Ran, Silvana Konermann, Vineeta Agarwala, Yingqing Li, Eli J. Fine, Xuebing Wu, Ophir Shalem, Thomas J. Cradick, Luciano A. Marraffini, Gang Bao, Feng Zhang, DNA targeting specificity of RNA-guided Cas9 nucleases, *Nat. Biotechnol.* 31 (2013) 827–832.
- [41] G. Jason, M.M. Fewell, Gregory Slobodkin, Sang-Oh Han, Jennifer Rice, Bruce Hovanes, Danny H. Lewis, Khursheed Anwer, Synthesis and application of a non-viral gene delivery system for immunogene therapy of cancer, *J. Control Release* 109 (2005) 288–298.
- [42] H. Cao, J. Chen, M. Avoniyi, J.R. Henley, M.A. McNiven, Dynamin 2 mediates fluid-phase micropinocytosis in epithelial cells, *J. Cell Sci.* 120 (2007) 4167–4177.
- [43] Z. Li, Y. Wang, J. Qiu, Q. Li, C. Yuan, W. Zhang, et al., The polycomb group protein EZH2 is a novel therapeutic target in tongue cancer, *Oncotarget* 4 (2013) 2532–2549.
- [44] Y. Zhang, W. Gong, S. Dai, G. Huang, X. Shen, M. Gao, et al., Downregulation of human farnesoid X receptor by miR-421 promotes proliferation and migration of hepatocellular carcinoma cells, *Mol. Cancer Res. MCR* 10 (2012) 516–522.
- [45] L. Cong, F.A. Ran, D. Cox, S. Lin, R. Barretto, N. Habib, et al., Multiplex genome engineering using CRISPR/Cas systems, *Science* 339 (2013) 819–823.
- [46] E. Basner-Tschakarjan, A. Mirmohammadsadegh, A. Baer, U.R. Hengge, Uptake and trafficking of DNA in keratinocytes: evidence for DNA-binding proteins, *Gene Ther.* 11 (2004) 765–774.
- [47] A.M. Goodwin, In vitro assays of angiogenesis for assessment of angiogenic and anti-angiogenic agents, *Microvasc. Res.* 74 (2007) 172–183.
- [48] O. Uluckan, A. Segaliny, S. Botter, J.M. Santiago, A.J. Mutsaers, Preclinical mouse models of osteosarcoma, *BoneKEy Rep.* 4 (2015) 670.
- [49] E. Ortiz-Zapater, D. Pineda, N. Martinez-Bosch, G. Fernandez-Miranda, M. Iglesias, F. Alameda, et al., Key contribution of CPEB4-mediated translational control to cancer progression, *Nat. Med.* 18 (2011) 83–90.
- [50] A.A. Sabile, M.J. Arlt, R. Muff, B. Bode, B. Langsam, J. Bertz, et al., Cyr61 expression in osteosarcoma indicates poor prognosis and promotes intratibial growth and lung metastasis in mice, *J. Bone Miner. Res. Off. J. Am. Soc. Bone Miner. Res.* 27 (2012) 58–67.
- [51] Z. Tahergorabi, M. Khazaei, A review on angiogenesis and its assays, *Iran. J. Basic Med. Sci.* 15 (2012) 1110–1126.
- [52] K.R. Weiss, G.M. Cooper, J.A. Jadlowiec, R.L. McGough 3rd, J. Huard, VEGF and BMP expression in mouse osteosarcoma cells, *Clin. Orthop. Relat. Res.* 450 (2006) 111–117.
- [53] W.M. Rockey, F.J. Hernandez, S.Y. Huang, S. Cao, C.A. Howell, G.S. Thomas, et al., Rational truncation of an RNA aptamer to prostate-specific membrane antigen using computational structural modeling, *Nucleic Acid. Ther.* 21 (2011) 299–314.
- [54] A.D. Keefe, S. Pai, A. Ellington, Aptamers as therapeutics, *Nat. Rev. Drug Discov.* 9 (2010) 537–550.
- [55] J.C. Gilbert, T. DeFeo-Fraulini, R.M. Hutabarat, C.J. Horvath, P.G. Merlini, H.N. Marsh, et al., First-in-human evaluation of anti von Willebrand factor therapeutic aptamer ARC1779 in healthy volunteers, *Circulation* 116 (2007) 2678–2686.
- [56] J. Wang, Z. Lu, Y. Gao, M.G. Wientjes, J.L. Au, Improving delivery and efficacy of nanomedicines in solid tumors: role of tumor priming, *Nanomedicine* 6 (2011) 1605–1620.
- [57] I.A. Khalil, K. Kogure, S. Futaki, H. Harashima, High density of octaarginine stimulates macropinocytosis leading to efficient intracellular trafficking for gene expression, *J. Biol. Chem.* 281 (2006) 3544–3551.
- [58] N. Feng, Z. Wang, Z. Zhang, X. He, C. Wang, L. Zhang, miR-487b promotes human umbilical vein endothelial cell proliferation, migration, invasion and tube formation through regulating THBS1, *Neurosci. Lett.* 591 (2015) 1–7.
- [59] M. Baker, S.D. Robinson, T. Lechertier, P.R. Barber, B. Tavora, G. D'Amico, et al., Use of the mouse aortic ring assay to study angiogenesis, *Nat. Protoc.* 7 (2011) 89–104.
- [60] W. Song, C.W. Fhu, K.H. Ang, C.H. Liu, N.A. Johari, D. Lio, et al., The fetal mouse metatarsal bone explant as a model of angiogenesis, *Nat. Protoc.* 10 (2015) 1459–1473.
- [61] S.-D. Li, Tumor-targeted delivery of siRNA by self-assembled nanoparticles, *Mol. Ther.* 16 (2008) 163–169.
- [62] G. Zhang, B. Guo, H. Wu, T. Tang, B.T. Zhang, L. Zheng, et al., A delivery system targeting bone formation surfaces to facilitate RNAi-based anabolic therapy, *Nat. Med.* 18 (2012) 307–314.
- [63] R. Shi, J. Li, F. Tang, Y.I. Luo, C.Q. Tu, Identification and functional study of osteosarcoma metastasis marker genes, *Oncol. Lett.* 10 (2015) 1848–1852.
- [64] T. Scholzen, J. Gerdes, The Ki-67 protein: from the known and the unknown, *J. Cell. Physiol.* 182 (2000) 311–322.
- [65] K.W. Hunter, Ezrin, a key component in tumor metastasis, *Trends Mol. Med.* 10 (2004) 201–204.
- [66] A. Merdad, S. Karim, H.J. Schulten, A. Dallol, A. Buhmeida, F. Al-Thubaity, et al., Expression of matrix metalloproteinases (MMPs) in primary human breast cancer: MMP-9 as a potential biomarker for cancer invasion and metastasis, *Anticancer Res.* 34 (2014) 1355–1366.
- [67] A.C. Mita, M.M. Mita, S.T. Nawrocki, F.J. Giles, Survivin: key regulator of mitosis and apoptosis and novel target for cancer therapeutics, *Clin. Cancer Res. Off. J. Am. Assoc. Cancer Res.* 14 (2008) 5000–5005.
- [68] A.M. Muller, M.I. Hermanns, C. Skrzynski, M. Nesslinger, K.M. Muller, C.J. Kirkpatrick, Expression of the endothelial markers PECAM-1, vWF, and CD34 in vivo and in vitro, *Exp. Mol. Pathol.* 72 (2002) 221–229.
- [69] G. McMahon, VEGF receptor signaling in tumor angiogenesis, *Oncologist* 5 (Suppl 1) (2000) 3–10.
- [70] H.X. Chen, R.E. Gore-Langton, B.D. Cheson, Clinical trials referral resource: current clinical trials of the anti-VEGF monoclonal antibody bevacizumab, *Oncology* 15 (2001), 1017, 20, 23–26.
- [71] D.C. Turner, F. Navid, N.C. Daw, S. Mao, J. Wu, V.M. Santana, et al., Population pharmacokinetics of bevacizumab in children with osteosarcoma: implications for dosing, *Clin. Cancer Res. Off. J. Am. Assoc. Cancer Res.* 20 (2014) 2783–2792.
- [72] T. Kamba, D.M. McDonald, Mechanisms of adverse effects of anti-VEGF therapy for cancer, *Br. J. Cancer* 96 (2007) 1788–1795.
- [73] L. Li, L. Song, X. Liu, X. Yang, X. Li, T. He, et al., Artificial virus delivers CRISPR-Cas9 system for genome editing of cells in mice, *ACS Nano* 11 (2017) 95–111.
- [74] B.J. Baaten, C.R. Li, L.M. Bradley, Multifaceted regulation of T cells by CD44, *Commun. Integr. Biol.* 3 (2010) 508–512.
- [75] L. Li, Z.Y. He, X.W. Wei, G.P. Gao, Y.Q. Wei, Challenges in CRISPR/CAS9 delivery: potential roles of nonviral vectors, *Hum. Gene Ther.* 26 (2015) 452–462.
- [76] Y. Yang, L. Wang, P. Bell, D. McMenamin, Z. He, J. White, et al., A dual AAV system enables the Cas9-mediated correction of a metabolic liver disease in newborn mice, *Nat. Biotechnol.* 34 (2016) 334–338.
- [77] H. Yin, C.Q. Song, J.R. Dorkin, L.J. Zhu, Y. Li, Q. Wu, et al., Therapeutic genome editing by combined viral and non-viral delivery of CRISPR system components in vivo, *Nat. Biotechnol.* 34 (2016) 328–333.
- [78] K. Anwer, M.N. Barnes, J. Fewell, D.H. Lewis, R.D. Alvarez, Phase-I clinical trial of IL-12 plasmid/lipopolymer complexes for the treatment of recurrent ovarian cancer, *Gene Ther.* 17 (2010) 360–369.